Neuro-Oncology 15(5):515–534, 2013.
doi:10.1093/neuonc/nos307
Advance Access publication January 16, 2013

Differentiating tumor recurrence from treatment necrosis: a review of neuro-oncologic imaging strategies

Nishant Verma, Matthew C. Cowperthwaite, Mark G. Burnett, and Mia K. Markey

Department of Biomedical Engineering, The University of Texas at Austin, Austin, Texas (N.V.); NeuroTexas Institute, St. David's HealthCare, Austin, Texas (N.V., M.C.C., M.G.B.); Department of Biomedical Engineering, The University of Texas at Austin, Austin, Texas (M.K.M.); Department of Imaging Physics, The University of Texas MD Anderson Cancer Center, Houston, Texas (M.K.M.)

Differentiating treatment-induced necrosis from tumor recurrence is a central challenge in neuro-oncology. These 2 very different outcomes after brain tumor treatment often appear similarly on routine follow-up imaging studies. They may even manifest with similar clinical symptoms, further confounding an already difficult process for physicians attempting to characterize a new contrast-enhancing lesion appearing on a patient's follow-up imaging. Distinguishing treatment necrosis from tumor recurrence is crucial for diagnosis and treatment planning, and therefore, much effort has been put forth to develop noninvasive methods to differentiate between these disparate outcomes. In this article, we review the latest developments and key findings from research studies exploring the efficacy of structural and functional imaging modalities for differentiating treatment necrosis from tumor recurrence. We discuss the possibility of computational approaches to investigate the usefulness of fine-grained imaging characteristics that are difficult to observe through visual inspection of images. We also propose a flexible treatment-planning algorithm that incorporates advanced functional imaging techniques when indicated by the patient's routine follow-up images and clinical condition.

Keywords: functional imaging, neuro-oncology, pseudoprogression, tumor recurrence, treatment necrosis.

The current treatment regimen for patients with brain tumor typically involves a combination of surgery, radiation, and chemotherapy that is based on tumor histology and location. Radiation and chemotherapy can be used alone to eradicate malignant tumors or as adjuvant therapies to prevent recurrence after surgical resection of a tumor. Although these therapies are effective treatment for brain tumors, they also carry the risk of deleterious effects on the surrounding healthy tissue resulting in treatment-induced tissue necrosis. The appearance of treatment-induced tissue necrosis on conventional imaging and its associated clinical symptoms are very similar to brain tumor recurrence, and therefore, it is difficult to differentiate between the 2 outcome types during patient follow-up. Furthermore, a new contrast-enhancing lesion observed on follow-up imaging is often a mixture of necrotic tissue and growing tumor, and this adds to the complexity of lesion characterization. It is crucial for clinicians to be able to determine the etiology of a lesion observed on follow-up imaging because the management strategies for tumor recurrence and treatment necrosis are different. This information is also critical for providing vital prognostic information to patients.

Biopsy is the most reliable method for differentiating treatment necrosis from tumor recurrence; however, brain tumor biopsies are expensive and carry the risks associated with surgery. Furthermore, any surgical intervention further deteriorates the quality of life for patients already undergoing aggressive treatment of their primary cancer; in patients with treatment necrosis, a biopsy would pose an unnecessary risk and negatively impact their lives. Therefore, there is significant interest in developing noninvasive methods that could determine whether a contrast-enhancing area is attributable to treatment necrosis or tumor recurrence. Such methods could potentially reduce the number of surgeries

Received May 25, 2012; accepted November 5, 2012.

Corresponding author: Mia K. Markey, Department of Biomedical Engineering, The University of Texas at Austin, 107 W Dean Keeton, Austin, Texas, 78712 (mia.markey@utexas.edu).

performed on benign lesions, which would reduce health care costs, increase patient survival, and improve quality of life. In cases of severe radiation-induced necrosis that require surgery to reduce mass effect, noninvasive methods can be used to guide biopsy or tissue sample collection from the region. Several imaging techniques have been evaluated for this purpose. Structural imaging methods that primarily provide anatomical information, such as magnetic resonance imaging (MRI), are routinely used in the clinical setting to follow and monitor patients with brain tumor; however, they suffer from limitations in differentiating treatment necrosis from tumor recurrence.[1–7] Functional imaging techniques have been extensively investigated with high sensitivities reported for differentiating between tumor recurrence and treatment necrosis. The purpose of this review is to discuss the utility of structural and functional imaging with special focus on the limitations faced by these imaging techniques for accurately differentiating between tumor recurrence and treatment necrosis. We discuss the potential for quantitative analyses of fine-grained imaging characteristics that are difficult to observe by manual inspection of images to address this problem. We also propose a flexible treatment-planning algorithm for patients with brain tumor that uses functional imaging when indicated by routine follow-up images and the patient's clinical condition.

Treatment-Induced Tissue Necrosis and Pseudoprogression

Radiation therapy is an integral part of the current treatment regimen for brain tumors. Classically, the biological and clinical adverse effects of radiation therapy can be classified into 3 types based on time of occurrence and clinical presentation: acute, early-delayed, and late-delayed radiation damage.[8] Acute and early-delayed radiation effects occur within the first 3 months after initiation of radiation therapy and are associated with clinical symptoms, such as headache, nausea, and somnolence, which likely result from increased intracerebral pressure. These early radiation effects are believed to result from vasodilation, blood-brain barrier disruption, and edema.[9] Unlike acute effects, which typically do not manifest with abnormal findings on MRI, early-delayed effects may appear as nonenhancing white matter T2-signal hyperintensities and new or enhancing contrast-enhancing lesions in proximity to the irradiated tumor site on imaging.[1] Both acute and early-delayed effects typically spontaneously resolve and do not require additional treatment. The symptoms of acute and early-delayed radiation effects can often be effectively treated with corticosteroids, when necessary.

Late-delayed radiation effects, on the other hand, may occur 3 months to years after radiation treatment, are often progressive, and may require additional intervention to mitigate their effects.[10] Radiation necrosis is a common late-delayed radiation effect originating from severe brain tissue reaction to radiation therapy that results in endothelial apoptosis and neuroinflammation. It has increased incidence in white matter and manifests on conventional imaging similar to a malignant tumor with contrast enhancement, edema, and mass effect. The symptoms of radiation necrosis may significantly vary from being nearly asymptomatic to significant neurological deficits. The incidence of radiation necrosis is ~3%–24%, with its occurrence directly related to radiation dose, overall treatment duration, and irradiated brain volume.[8,11–14] A significant increase in the risk of developing treatment necrosis has been reported when the total radiation dose exceeds 64.8 Gy.[15] The concurrent and adjuvant use of chemotherapy has been shown to improve survival among patients with brain tumor. However, its concurrent use with radiation therapy has been reported to increase the risk of developing tissue necrosis by at least 3-fold.[12–14] This is partially attributable to the breakdown of blood-brain barrier by radiation injury, which enhances the effectiveness of chemotherapeutic agents and causes unintended injury to tissue surrounding tumor. However, the exact contribution of chemotherapy in developing tissue necrosis is unclear, and therefore, we refer to this combined effect of radiation and chemotherapy as treatment necrosis.

Similar to radiation necrosis, another clinical phenomenon that mimics early tumor recurrence on conventional imaging and presents a significant diagnostic dilemma to physicians is pseudoprogression. Pseudoprogression is defined as a transient period of apparent radiographic deterioration around the time when early-delayed radiation effects are expected. This may often get misinterpreted as early tumor recurrence. Pseudoprogression is also sometimes associated with worsening of neurological deficits, which further complicates its discrimination from early tumor recurrence. When using concurrent chemotherapies, such as temozolomide (TMZ), development of radiation necrosis is more likely and often occurs sooner during the early-delayed period. Therefore, researchers have interchangeably used the terms treatment necrosis and pseudoprogression in the literature. However, pseudoprogression is different from radiation necrosis, because these lesions and associated clinical symptoms recover spontaneously.[12,16]

Differentiating among treatment necrosis, pseudoprogression, and tumor recurrence is expected to become even more complicated as additional treatment modalities (such as immunotherapy, antivascular agents, and gene therapy) are included for brain tumor treatment. The addition of immunotherapy and chemical agents may enhance multiple apoptotic pathways through several metabolic pathways, resulting in an increased risk of developing treatment necrosis and pseudoprogression. This may be one of the reasons behind the higher incidence of treatment effects and pseudoprogression with multimodality therapies. The inclusion of additional treatment methods also reduces the specificity of contrast enhancement as a surrogate marker for

defining disease progression, thereby requiring appropriate adjustments in the imaging criteria, as discussed in the next section.

Structural Imaging

Structural imaging methods, such as MRI and CT, provide information about brain structure and are interpreted on the basis of observed gross anatomical changes. Structural imaging with and without contrast media is widely used in the clinical setting for treating patients with brain tumor.

MRI

MRI is the most widely used structural imaging technique for the initial diagnosis and follow-up monitoring of brain tumors because of its high sensitivity and ability to provide detailed information about brain structures. On MRI, malignant brain tumors are typically characterized by intravenous contrast enhancement, mass effect, and associated vasogenic edema.[17,18] However, treatment necrosis also presents with similar characteristics, making it difficult to reliably distinguish from tumor recurrence. Figure 1 shows the similar appearance of treatment necrosis and tumor recurrence on routinely collected structural MR sequences. Some of the imaging features most commonly reported to be shared by tumor recurrence and treatment necrosis include (1) origin near the primary tumor site, (2) contrast-agent enhancement, (3) vasogenic edema, (4) growth over time, and (5) mass effect.[1–3,19] Other less common features have also been reported to describe lesions stemming from treatment necrosis and tumor recurrence (Table 1). Features such as conversion from a nonenhancing to an enhancing lesion after radiation therapy,[1] lesions appearing distant from the primary resection site,[1] corpus-callosum or peri-ventricular white matter involvement,[1,3,19–24] and "Swiss cheese" or "soap bubble" shape patterns[1] have been suggested to favor treatment necrosis over tumor recurrence. However, others[2] failed to validate these findings and even reported some contradictory results. It has also been suggested that a combination of multiple features offers more statistical power than individual features.

Although several studies have reported features specific to either treatment necrosis or tumor recurrence, no feature or combination of features has been established as a reliable discriminator between these 2 outcomes. This suggests that MRI offers only limited power to differentiate between these 2 outcomes, because there is significant overlap among their gross radiologic features. However, the relatively small sample sizes that were used in most studies could explain some

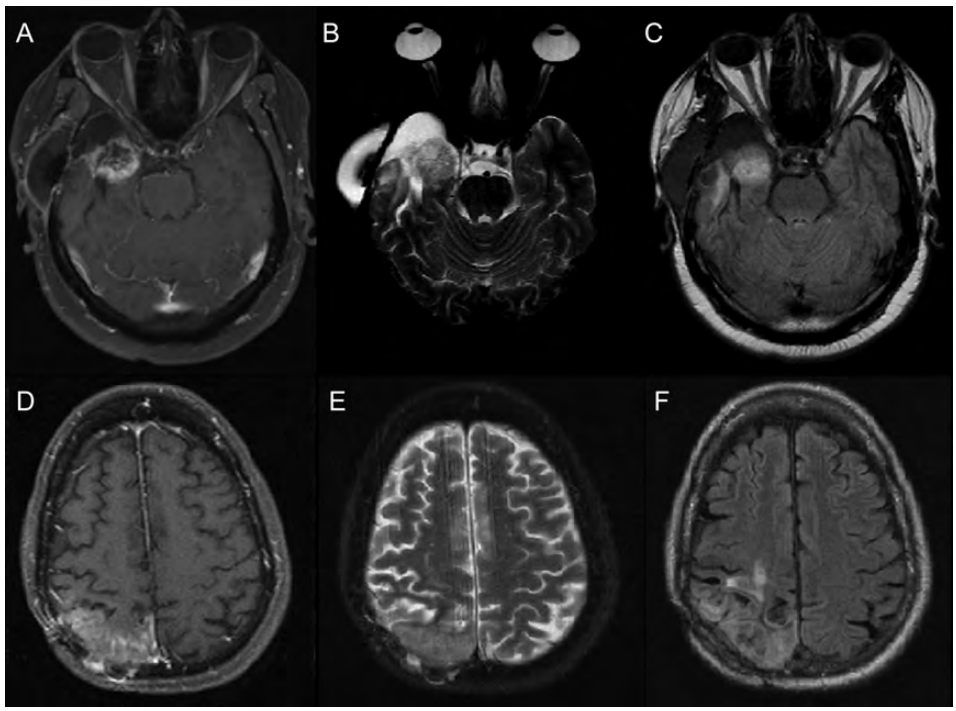

Fig. 1. Ambiguities involved in differentiating between tumor recurrence and treatment necrosis based on routinely collected structural imaging sequences: T1 with Gadolinium contrast (T1-post Gad), T2-weighted images, and fluid attenuated inverse recovery (FLAIR). (A, B, C) T1-post Gad, T2-weighted, and FLAIR images of histopathologically confirmed case of glioblastoma recurrence, respectively. The patient underwent surgical resection of right temporal lobe tumor, followed by combined temozolomide/radiation therapy. (D, E, F) T1-post Gad, T2-weighted, and FLAIR images of pathologically proven case of treatment necrosis. The patient underwent surgical resection of right parietal oligodendroglioma, followed by combined chemotherapy (Avastin) and radiation therapy.

Table 1. Structural imaging (MRI and CT) features reported for differentiation between treatment necrosis (TN) and recurrence tumor (RT).

Study	Features on structural imaging	Number of patients
Treatment necrosis		
Kumar et al.[1]	- Conversion from non-enhancing lesion before irradiation to enhancing focus post radiation therapy. - Enhancing focus at a distance from original glioma site. - Enhancement or no-enhancement in peri-ventricular white matter, particularly capping ventricles or within corpus callosum. - New enhancing lesion exhibiting soap bubble or Swiss cheese pattern.	36 (TN-20, RT+TN-16)
Curnes et al.[3]	- Scalloped appearance reflecting damage throughout the white matter including the arcuate (U) fibers. - Asymmetric less extensive irregular peri-ventricular signal.	9 (TN)
Chan et al.[19]	- Extent of white matter lesions greater than that of gray matter lesions. - Blood brain barrier disruption based on parenchymal contrast enhancement. - Hemosiderin deposition.	34 (TN)
Tsuruda et al.[22]	- High signal symmetric foci in the periventricular, supratentorial white matter. - Often remote from tumor site.	95 (TN)
Tumor Recurrence		
Mullins et al.[2]	- Multiple enhancing lesions + corpus callosum involvement with sub-ependymal spread. - Involvement of corpus callosum with crossing of the midline + multiple enhancing lesions.	27 (RT-15, TN-12)

*RT+TN indicates lesions with a mixture of RT and TN.

of the inconsistencies across studies; future studies should use larger sample sizes to identify features that can distinguish between tumor recurrence and treatment necrosis and validate their statistical significance. Moreover, the confounding effects of additional treatment modalities, such as immunotherapy, antivascular therapy, and gene therapy, must be considered when investigating image features for differentiating between tumor recurrence and treatment necrosis. These affect the degree of contrast enhancement observed on MRI and may result in misdiagnosis of tumor recurrence, a phenomenon often termed pseudoresponse.

The limited power of structural MRI in differentiating among clinical phenomena, such as pseudoprogression, tumor progression/recurrence, and pseudoresponse, have highlighted some limitations of the Macdonald criteria,[25] which is the most widely used criteria for determining tumor response and progression after therapy. An international effort by the Response Assessment in Neuro-Oncology working group recently updated the Macdonald criteria to address some of these limitations. To avoid misinterpretation of pseudoprogression as early tumor recurrence, the updated criteria define disease progression (tumor recurrence) within the first 3 months (early-delayed time period) only if the new enhancement is observed outside the radiation field or if any histopathological confirmation exists.[26] Likewise, to avoid misdiagnosis of tumor recurrence during anti-angiogenic therapy, the updated criteria define disease progression as the enlargement of nonenhancing T2-hyperintense lesions.[26] Despite these modifications, the ability of imaging criteria to accurately differentiate between tumor recurrence and treatment necrosis is limited because of the overlap in their MRI features and time of occurrence. The inclusion of clinical data and functional imaging techniques in this criterion may potentially help improve specificity in the detection of tumor recurrence.

CT

CT also suffers from similarity of gross characteristics between the 2 outcome types.[4–6] The following characteristics have been reported to characterize both radiation-induced adverse effects and tumor recurrence on CT: (1) diffuse hypo-intensity of the white matter extending into and compressing the overlying cortex likely caused by edema, (2) enhancing focal areas of lucency suggesting necrosis, (3) irregular and/or extensive contrast enhancement, and (4) mass effect.[5,7] Moreover, in metastatic tumors, the size of postsurgical contrast-enhanced regions may not increase over time and, as a result, may be misinterpreted as a case of treatment necrosis when it is in fact tumor recurrence.[27–30] Therefore, CT remains limited both by its relatively low power to differentiate between treatment necrosis and tumor recurrence and its use of ionizing radiation that generates patient safety concerns.

Functional Imaging

Functional imaging has been extensively evaluated for differentiating between tumor recurrence and treatment

necrosis. We review some of the most commonly studied functional imaging methods with an emphasis on their accuracy, advantages, and limitations when distinguishing between these 2 etiologies.

Diffusion Imaging

Diffusion imaging captures the Brownian motion of water molecules inside brain volumes that can be used to describe the structure of the tissue at the cellular level. Diffusion weighted imaging (DWI) enables calculation of apparent diffusion coefficient (ADC), which represents the magnitude of water diffusion inside voxels. Diffusion tensor imaging (DTI) is a more sophisticated version of DWI that also measures the directionality of proton movement within each voxel in terms of fractional anisotropy (FA). In contrast to other functional imaging techniques that are seldom used in the clinic, diffusion imaging is routinely used in combination with structural imaging for both diagnosing and following up patients with brain tumor. Here, we review parameters obtained from diffusion imaging and discuss their use in differentiating treatment necrosis from tumor recurrence.

ADC

ADC estimates the mean diffusivity of water molecules within each voxel (in mm^2/s), assuming isotropy along each direction of movement.[31–34] The movement of water molecules can be restricted by several intracellular structures, such as membranes, organelles, and cytoskeletal components, and therefore, water molecules diffuse more slowly in intracellular space than in extracellular space. Pathological processes, such as tumor growth, edema, and necrosis, result in the loss of intracellular structures and, therefore, elevate ADC values relative to normal brain tissue.[32,35,36] Tumor recurrence has greater cellularity than treatment necrosis, and therefore, lower ADC values are expected, compared with treatment necrosis. However, the ADC values reported thus far are somewhat inconsistent (Table 2). The majority of studies have reported lower ADC values in tumor recurrence than in treatment necrosis.[31,32,37–41] However, one study reported significantly higher ADC values in tumor recurrence than in treatment necrosis,[42] which could be attributable to greater extracellular space or necrotic regions within high-grade tumors. The ADC values in treatment necrosis can also be lower because of scarring (from gliosis or fibrosis) within the lesion, whereas edema can elevate the ADC values,[42,43] possibly because of pure vasogenic edema, which would have greater water-molecule mobility, compared with edema associated with tumor recurrence. The effects of infiltration and proliferation have also been noted to confound the straightforward interpretation of ADC values.[44] Mean ADC values inside the lesion have limitations in differentiating among pure tumor recurrence, pure treatment necrosis, and mixture of both etiology types. However, ADC histogram analysis may reveal additional information that can help identify a mixture of necrosis and recurrence. Figure 2A shows an ADC map with marked region of

Table 2. Reported diffusion ADC and FA parameter values (mean ± standard deviation) and significance levels (*P* value) in differentiating between treatment necrosis (TN) and recurrent tumor (RT)

Study	Diffusion parameters	TN	RT	*P* value	Number of patients
Sundgren et al.[42]	ADC value in lesion	1.12 ± 0.14	1.27 ± 0.15	0.01	26 (RT-14, TN-12)
	FA value in lesion	0.17 ± 0.04	0.15 ± 0.05	0.13	
	FA ratios in NAWM	0.89 ± 0.15	0.74 ± 0.14	0.03	
	ADC ratios in perilesional edema	1.85 ± 0.30	1.60 ± 0.27	0.09	
Kashimura et al.[47] (Case study)	FA value: case 1	-	0.27 ± 0.04	-	3 (RT-2, TN-1)
	FA value: case 2	-	0.29 ± 0.04	-	
	FA value: case 3	0.17 ± 0.03	-	-	
Hein et al.[31]	ADC ratios	1.82 ± 0.07	1.43 ± 0.11	<0.001	18 (RT-12, TN-6)
	Mean ADC values	1.40 ± 0.17	1.18 ± 0.13	<0.006	
Xu et al.[37]	ADC values in lesion	1.54 ± 0.17	1.23 ± 0.20	0.0002	35 (RT-20, TN-15)
	ADC values in edema	1.28 ± 0.37	1.52 ± 0.34	0.0564	
	Mean ADC ratios in lesion	1.62 ± 0.17	1.34 ± 0.15	0.0013	
	ADC ratios in edema	1.51 ± 0.19	1.68 ± 0.22	0.0643	
	FA values in lesion	0.14 ± 0.03	0.24 ± 0.05	0.0025	
	FA values in edema	0.29 ± 0.05	0.33 ± 0.03	0.0568	
	Mean FA ratios in lesion	0.32 ± 0.03	0.45 ± 0.03	0.0015	
	FA ratios in edema	0.55 ± 0.04	0.59 ± 0.02	0.0732	
Zeng et al.[39]	ADC values	1.39 ± 0.09	1.20 ± 0.08	<0.01	55 (RT-32, TN-23)
	ADC ratios	1.69 ± 0.08	1.42 ± 0.10	<0.01	
Asao et al.[38]	Maximal ADC	2.30 ± 0.73	1.68 ± 0.37	0.039	17 (RT-5, TN-12)
	Minimal ADC	1.04 ± 0.31	1.07 ± 0.18	>0.05	
	Mean ADC	1.68 ± 0.46	1.37 ± 0.25	>0.05	
Rock et al.[32]	ADC	ADC > 1.60	ADC<1.30	0.1263	18 (RT-12, TN-6)
Matsusue et al.[53]	ADC ratio	1.57 ± 0.35	1.14 ± 0.18	<0.05	15 (RT-10, TN-5)

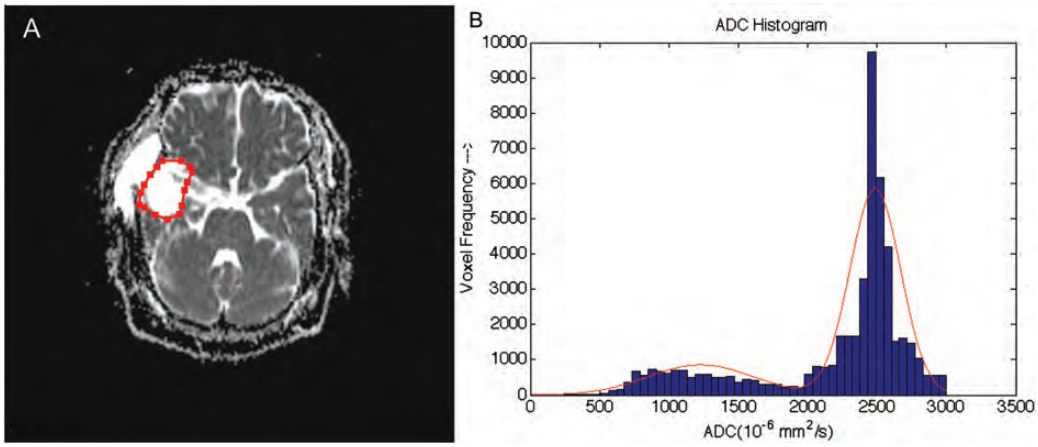

Fig. 2. The usefulness of ADC histogram analysis in differentiating among pure tumor recurrence, pure treatment necrosis, and mixture of 2 etiology types. (A) ADC map with labeled region of interest (ROI) outlining the lesion extent determined using structural images. (B) ADC histogram with a 2-component normal mixture model fitted to the data (shown in red curve). The patient underwent surgical resection of right temporal lobe glioblastoma, followed by combined temozolomide/radiation therapy. High ADC values in the temporal lobe and low choline with use of MR spectroscopy suggested treatment necrosis; however, the pathological verification confirmed tumor recurrence.

interest outlining the lesion extent on the image slice, which is determined using structural images. High ADC values and low choline peak observed on MR spectroscopy led to a misinterpretation of treatment necrosis; the case was later pathologically confirmed to contain tumor recurrence. The low choline and high ADC values can be attributable to a mixture of recurrence and treatment necrosis present inside the lesion. An ADC histogram fitted with a 2-component normal mixture model reveals 2 centers (Fig. 2B), corresponding to tumor recurrence and treatment necrosis.

FA

FA captures the directionality of diffusion inside the tissue.[35,42,43,45–47] FA values are typically high in healthy, normal white matter, because water molecules rapidly diffuse parallel to the white matter tracts.[48] White matter abnormalities that cause the loss of axonal organization produce lower FA and higher ADC values.[46,48] However, other factors, such as vascularity, cellular density, and fiber structure, can also affect FA values. Although FA values have been used to differentiate among different tumor grades,[33,34] few studies justify its use for differentiating tumor recurrence from treatment necrosis. Generally, lower FA values are expected in a growing tumor, in which the surrounding fibers and supporting cells are disrupted, thereby altering water diffusion; however, higher FA values have been reported to characterize high-grade tumors.[35,45] Treatment necrosis, which causes loss of cell structures and normal fibers, should produce even lower FA values than should tumor recurrence. A case report by Kashimura et al.[47] reported lower FA value (0.17) in a case of treatment necrosis than 2 cases of tumor recurrence (0.29 and 0.27). Xu et al.[37] reported similar findings in a later study. In contrast, Sundgren et al.[42] reported no significant differences in FA values between tumor recurrence and treatment necrosis, although it was observed that the FA values in the normal-appearing white matter adjacent to perilesional edema were higher in recurrent tumors than in treatment necrosis. This possibly resulted from pure vasogenic edema in treatment necrosis having greater isotropic water diffusion than the edema associated with recurrent tumor.

Diffusion imaging largely remains in an exploratory stage, and its potential clinical usefulness for differentiating between tumor recurrence and treatment necrosis remains to be comprehensively evaluated. As such, the technology has several limitations that must be overcome before it can be routinely used in clinical practice. First, the measurements obtained, especially ADC values, significantly vary with scanner type and magnetic field strength.[31,32,37–39,42,47] Some studies have proposed normalizing lesion ADC values relative to the ADC values in the surrounding normal tissue; however, significant variations in ADC ratios have still been reported across different studies when incorporating this correction. Therefore, it will be difficult to establish a universal threshold that differentiates treatment necrosis from tumor recurrence. One important source of variation when estimating ADC is diffusion weighting, or the b-value. Typically, 2 b-value images are required to estimate ADC inside the voxels. The use of very low (<200 s/mm^2) and very high b-values (>2000 s/mm^2) is discouraged for ADC estimation.[49,50] A low b-value introduces perfusion errors that result in overestimation of the ADC values. A high b-value, on the other hand, is theoretically more desirable for obtaining better contrast and is feasible by moderate increases in the echo time (TE) because of its (time)^3 dependence. However, the signal-to-noise ratio (SNR) becomes a limiting factor because of signal loss at high b-values, and therefore, moderately high b-values are recommended ($\sim$1000 s/mm^2). Uniformity of the

b-values from different acquisitions is important to ensure the standardization of the estimated ADC values.[51] In contrast, no significant changes in FA values are observed when different b-values are considered.[52]

Second, the effects of common processes, such as necrosis, gliosis, fibrous scar tissue formation, and tissue granulation on ADC or FA values, are not well understood. DTI also estimates FA and has shown promise in differentiating between treatment necrosis and tumor recurrence. However, further investigations with larger sample sizes are required to validate the use of FA for this application. Third, there are limitations for diffusion imaging to resolve lesions with a mixture of recurrence and treatment necrosis, because the mean ADC and FA values are easily skewed, which may result in misinterpretation. This can potentially be dealt with by increasing the b-value, which improves the contrast resolution to detect subtle differences in diffusion between regions of necrosis and recurrence inside the lesions. However, there is significant signal loss at higher b-values, which typically has to be compensated for by decreasing spatial resolution. Additional serious limitations that need to be considered are the long scan times, low SNR, and inferior resolution of diffusion imaging.

Perfusion Imaging

MR Perfusion

The use of perfusion imaging as a tool to differentiate between tumor recurrence and treatment necrosis has been explored.[53–60] Tumor recurrence is associated with the formation of complex networks of abnormal blood vessels with increased permeability around the tumor site that appear as regions of hyperperfusion with higher blood volume. Treatment necrosis, on the other hand, is associated with regions of reduced perfusion because of treatment-induced vascular endothelial damage and coagulative necrosis. The following sections focus on the application of the 2 most widely used MR perfusion methods: dynamic susceptibility-weighted contrast-enhanced (DSC) MR imaging and dynamic contrast-enhanced (DCE) MR imaging for differentiating between tumor recurrence and treatment necrosis.

DSC MR Imaging.—DSC-MRI relies on the T2* signal drop caused by the susceptibility effect of gadolinium-based contrast agents in brain tissue. The drop in signal correlates with the concentration of the contrast agent and can be used to measure the hemodynamic parameters. The hemodynamic characteristics of the tissue are quantified using 3 measures: relative cerebral blood volume (rCBV), relative peak height (rPH), and percentage of signal-intensity recovery (PSR).

rCBV. rCBV has been consistently reported to be promising for differentiating between tumor recurrence and treatment necrosis (Table 3).[58,61,62] Abnormal and highly permeable blood vessels growing around the site of a recurrent tumor result in higher rCBV values than in normal brain tissue.[54–56,58,63,64] In contrast, treatment necrosis hinders blood flow and is associated with lower rCBV values. Kim et al.[54] and Prat et al.[65] reported that DSC-MRI using rCBV is superior to PET for differentiating tumor recurrence from treatment necrosis; however, additional studies are needed to validate these findings.

rPH. rPH is defined as the maximum change in signal intensity during the transit period of a contrast agent. rPH can be used to quantitatively measure tumor vasculature and has been reported to strongly correlate with rCBV.[56,61,62] Higher rPH values are expected to be associated with tumor recurrence, because progressing tumors have greater vasculature than does treatment necrosis. rPH has been used in conjunction with rCBV to differentiate between tumor progression and treatment necrosis.[55,56]

PSR. PSR measures the degree of contrast agent leakage through the tumor microvasculature and, thus, directly reflects capillary permeability. Growing tumors recruit abnormally formed and leaky blood vessels that are expected to increase vascular permeability and, thus, lower PSR values. PSR should therefore be lower in tumor recurrence than in treatment necrosis, and it has been suggested to be the most powerful perfusion imaging variable for distinguishing tumor recurrence from treatment necrosis.[55,56] Two separate studies reported high sensitivity and specificity using PSR for differentiating tumor recurrence from treatment necrosis.[55,56] The quantification of microvasculature leakage also provides important insight into underlying biology of a growing tumor.[56,66]

Other parameters, such as lesion enhancement rate, have been less widely investigated to differentiate between tumor recurrence and treatment necrosis.[54,59] In comparison to other MR perfusion techniques, DSC-MRI has several advantages, such as better SNR, shorter scan times, ease of use, and greater availability in commercial scanners. These advantages make DSC-MRI the most widely used perfusion technique for the brain. The DSC-MRI hemodynamic parameters are typically obtained from the integral of the time susceptibility curve or by fitting a gamma-variate function, which eliminates the tracer recirculation effects. However, breakdown of the blood-brain barrier introduces errors in the calculation of the hemodynamic parameters. To reduce such errors, the pulse sequence parameters are often optimized to minimize the T1 effects.[67] DSC-MRI has been extensively studied and is reported to have promise for differentiating between tumor recurrence and treatment necrosis. Although DSC-MRI has several advantages over other MR perfusion techniques, it suffers from being highly sensitive to susceptibility artifacts, and therefore, its application in patients with hemorrhages, calcifications, or surgical clips is limited.

Table 3. Reported hemodynamic parameters (mean ± standard deviation), significance levels (*P* value), and accuracy (sensitivity, specificity) for differentiating between treatment necrosis (TN) and recurrent tumor (RT).

Study	Hemodynamic Parameters					Sensitivity	Specificity	Number of patients
	Parameter	Cutoff	RT	TN	*P*-value			
Sugahara et al.[58]	Normalized rCBV	1.0	2.51 ± 1.47	1.29 ± 0.71	0.03	50%	90%	20 RT-10 TN-10
Barajas et al.[56]	rCBV rPH PSR	1.54 0.69 76.3%	2.38 ± 0.95 1.58 ± 0.55 60.6 ± 9.95	1.54 ± 0.92 1.03 ± 0.49 83.3 ± 3.59	0.024 <0.01 <0.01	91.3% 86.96% 95.65%	72.73% 45.45% 100%	27 (30 lesions) RT-20* TN-10*
Kim et al.[54]	rCBV ratio	3.69	5.72 ± 2.53	2.53 ± 0.81	0.010	100%	100%	10 RT-4 TN-6
Barajas et al.[55]	rCBV rPH rPSR	1.75 1.38 87.3%	2.38 ± 0.87 2.07 ± 0.69 80.2 ± 10.3	1.57 ± 0.67 1.25 ± 0.42 89.3 ± 12.4	<0.01 <0.01 <0.05	78.92% 89.32% 78.26%	71.58% 81.38% 76.19%	57 TN-17 RT-40
Jain et al.[78]	nCBV nCBF nMTT	1.65 1.28 1.44	2.65 ± 0.28 2.73 ± 0.38 0.71 ± 0.08	1.10 ± 0.1 1.08 ± 0.11 1.58 ± 0.15	<0.001 <0.001 <0.001	83.3% 94.4% 94.4%	100% 87.5% 75%	22 TN-8 RT-14
Ozsunar et al.[63]	DSCE-CBV	*Based on visual inspection*				86%	70%	32 TN-12 RT-23
Matsusue et al.[53]	rCBV ratio	2.1	3.33 ± 1.16	1.82 ± 0.79	<0.05	90%	80%	15 TN-5 RT-10
Hazle et al.[59]	MER	-	5.85 ± 1.78 2.79 ± 1.03 8.62 ± 2.76 4.05 ± 1.36	1.90 ± 0.78	<0.05	-	-	95 TN-32 RT-63
Mitsuya et al.[57]	rCBV ratio	2.1	2.1–10	0.39–2.5	<.0001	100%	95.2%	27 (28 lesions) TN-21* RT-7*
Huang et al.[137]	rCBV	2	2.49 ± 1.73	1.03 ± 0.23	.02	56%	100%	26 (33 lesions) TN-10* RT-23*

Second column lists the cutoff values of hemodynamic parameters considered in these studies for differentiating between RT and TN.
Abbreviation: MER, maximum enhancement rate.
*count indicates number of lesions.

DCE MR Imaging.—DCE-MRI uses a rapid sequence of T1-weighted images to measures changes in signal intensity as a bolus of contrast agent passes through a brain tumor. The tumor signal intensity in DCE-MRI reflects a combination of factors, including overall perfusion, vascular permeability, and extracellular volume. The following quantitative hemodynamic parameters are measured in DCE-MRI: volume transfer of contrast between the blood plasma and extracellular space (K^{trans}), extravascular extracellular space (V_e), and area under the curve (iAUC). There are very few reports in the literature that describe the application of DCE-MRI to the problem of differentiating between tumor recurrence and treatment necrosis.[68,69] K^{trans} represents the permeability of the tumor vasculature and has been shown to be higher in tumor recurrence than in treatment necrosis.[68] Some non–model-based semiquantitative indices derived from DCE-MRI have been reported to attain statistical significance when differentiating between tumor recurrence and treatment necrosis.[69] Although it is difficult to derive a physiological basis for these indices, a direct correlation with K^{trans} has been reported.[70] iAUC provides insight into the kinetics of contrast agent accumulation by integrating the concentration of the agent observed in brain tissue over time. Because of the vascular dilation present in treatment necrosis, the iAUC values have been reported to be higher for treatment necrosis than for tumor recurrence. Extracellular volume (V_e) has also been investigated, but no statistically significant differences have been reported between the 2 lesion types.[68]

The quantification of hemodynamic parameters in DCE-MRI is complex and error prone,[71,72] mostly because of the nonlinear relationship between the T1-weighted signal intensity and contrast agent concentration[71,73–75] and the complex pharmokinetic models required for estimating these parameters. The most widely used model is the Tofts-Kermode model;[72] however, this model results in significant errors when estimating the hemodynamic parameters because of the incorrect assumption that the observed signal changes are a direct result of extravasated contrast agent within the extracellular space. Currently, no Food and Drug

Administration–approved commercial software exists for quantification of DCE-MRI parameters. This is a big hurdle in the application of DCE-MRI for clinical neuroimaging purposes. Another problem that limits the use of DCE-MRI for clinical neuroimaging is the poor temporal resolution and limited region of lesion coverage because of the short acquisition times. The pilot studies investigating the use of DCE-MRI have shown promise for differentiating between tumor recurrence and treatment necrosis. In addition to its limitations, DCE-MRI has some advantages over the more widely used DSC-MRI, such as better spatial resolution that allows more accurate characterization of the vascular microenvironment of the lesion and robustness to the presence of susceptibility artifacts. The higher spatial resolution is significant for resolving cases with a mixture of recurrence and treatment necrosis.

CT Perfusion

CT perfusion has been reported to differentiate tumor recurrence from treatment necrosis with reasonable accuracy.[76–78] It has some advantages over MR imaging: (1) CT scanners are more widely available; (2) unlike MR scanners, CT scanners do not suffer from magnetic susceptibility artifacts; and (3) CT is less prone to errors when quantifying hemodynamic parameters because of the linear relationship between tissue attenuation and contrast agent concentration and the presence of an arterial input function. CT perfusion has been reported to be promising for differentiating tumor recurrence from treatment necrosis; however, its clinical use remains limited because of its use of ionizing radiation, the toxicity associated with the iodinated contrast agents, lower resolution, and limited image-slice volumes. MR perfusion can be easily obtained as an additional sequence to a standard structural MRI. Perfusion CT, on the other hand, would require an additional imaging session in a different scanner, and these requirements further limit its feasibility for use in the clinical setting. CT perfusion is also incapable of imaging regions outside the preselected slice(s), and therefore, the data obtained from a single scan do not permit reconstruction of other imaging planes for a more detailed study; PET or MR perfusion does not suffer from this problem.

Magnetic Resonance Spectroscopy

Magnetic resonance spectroscopy (MRS) measures the relative compositions of various metabolites, most commonly including N-acetylaspartate (NAA), choline, creatine, lipid, and lactate. ^{1}H is the most commonly used nuclei in MRS, because it provides a much higher SNR than do other nuclei (e.g. ^{23}Na and ^{31}P). MRS has been widely used to grade tumors; the grades based on MRS signals have been reported to correlate with histological outcomes.[65,79–81] A malignant tumor is often associated with lower levels of NAA and creatine, higher levels of choline and lactate, and different lipid compositions, compared with normal tissue.[65,81–84] MRS has been reported to be particularly promising for differentiating between treatment necrosis and tumor recurrence. Early MRS had low spatial resolution and an inability to accurately classify cases of mixed tumor recurrence and treatment necrosis;[32,85–89] however, multivoxel approaches (chemical shift imaging) appear to more accurately differentiate tumor recurrence from treatment necrosis.[32,88–92]

NAA, Choline, and Creatine Ratios

MRS (Table 4) has been reported to accurately classify lesions as treatment necrosis or tumor recurrence on the basis of the ratios of NAA, choline, and creatine. Several studies have reported significantly higher choline to creatine and choline to NAA ratios in tumor recurrence than either the surrounding normal white matter or lesions resulting from treatment necrosis;[39,81,86,91,93,94] other studies have reported that NAA to creatine ratios are lower with recurrent tumor than normal appearing white matter.[39,86,91,93,95] Treatment necrosis, on the other hand, has been reported to show decreased NAA and variable changes in choline and creatine intensities over time.[32,85–88,96–99] For example, choline has been reported to increase during the first few months after radiation therapy[98,99] and then decrease as treatment necrosis begins to appear.[32] The few multivoxel studies conducted thus far have reported abnormal metabolic spectra beyond the contrast enhanced area[90,91,100,101] that may be useful for detecting the extent of tumor infiltration into the surrounding brain tissue. Such information could be used to customize a patient's treatment plan and would be extremely useful for more targeted radiation therapy to reduce the risk of undesirable treatment necrosis.

Lipid and Lactate

Lipid and lactate are released with cell destruction and, therefore, are typically absent in normal brain tissue. The ability of lipid and lactate concentration to differentiate between tumor recurrence and treatment necrosis has been investigated, with variable success being reported in literature. An increased amount of lipid and lactate can be found inside regions of treatment necrosis, when compared with pure tumor recurrence with no necrosis. However, a recurrent tumor often contains areas of necrosis and, therefore, shows elevated levels of lipid and lactate similar to treatment necrosis. A few studies have reported that lipid to creatine, lactate to creatine, and lactate to choline metabolite ratios can differentiate between tumor recurrence and treatment necrosis;[32,39,79,95] however, it is suspected that these studies considered only pure tumor recurrence, with no tissue necrosis in their studies. This suspicion is supported by studies that have reported no significant differences in signal intensities of lipid or lactate between tumor recurrence and treatment necrosis.[86,91] Cerebrospinal fluid and cysts can also contain lactate products and may

Table 4. Reported MR spectroscopy parameter values (mean ± standard deviation), significance levels (*P* value), and accuracy in differentiating between treatment necrosis (TN) and recurrent tumor (RT).

Study	Lesion type	Features of differentiation			Accuracy	Number of patients
		Cho/Cr	Cho/NAA	NAA/Cr		
Zeng et al.[39]	RT TN *P*-value	2 .82 ± 0.65 1.61 ± 0.34 <0.01	3.52 ± 0.98 1.55 ± 0.54 <0.01	0.84 ± 0.23 1.10 ± 0.26 <0.01	RT: 81.3% TN: 91.3% Total: 85.5%	55 RT-32 TN-23
Weybright et al.[91]	RT TN *P*-value	2.52 (1.66–4.26) 1.57 (0.72–1.76) <0.0001	3.48 (1.70–6.47) 1.31 (0.83–1.78) <0.0001	0.79 (0.47–1.15) 1.22 (0.94–1.69) <0.0001	RT: 93.75% TN: 100%	28 RT-16 TN-12
Smith et al.[93]	RT TN *P*-value	2.36 (1.30–4.26) 1.57 (0.72–2.70) <0.001	3.20 (1.30–6.47) 1.43 (0.83–2.40) <0.001	0.85 (0.47–1.23) 1.14 (0.50–1.69) 0.018	Cho/NAA: Sensitivity 85% Specificity 69.2%	33 RT-20 TN-13
Schlemmer et al.[86]	RT TN SD *P*-value	2.30 ± 1.29 1.26 ± 0.61 1.22 ± 0.50 <0.0001	3.44 ± 2.76 1.29 ± 1.17 1.24 ± 0.76 <0.0001	0.93 ± 0.81 1.31 ± 0.78 1.22 ± 0.53 0.0669	RT: 82% TN/SD: 81%	50 (66 lesions) RT-34* TN-17* SD-15*
Plotkin et al.[94]	RT TN *P*-value	1.38 ± 0.33 0.95 ± 0.34 0.030	1.51 ± 0.57 0.74 ± 0.24 <0.0001	0.99 ± 0.29 1.44 ± 0.77 0.212	Sensitivity 89% Specificity 83%	25 RT-19 TN-6
Ando et al.[138]	RT TN *P*-value	1.70 ± 0.96 1.04 ± 1.16 0.047	- - -	- - -	Sensitivity 64% Specificity 83%	20
Rock et al.[32]	RT TN *P*-value	>1.20 <1.20 0.0895	>0.20 <0.20 0.0714	<1.56 >1.56 0.0254	-	18 TN-6 RT-12
Zeng et al.[89]	RT TN *P*-value	2.62 ± 0.88 1.50 ± 0.15 <0.01	3.03 ± 1.19 1.42 ± 0.21 <0.01	0.89 ± 0.12 1.08 ± 0.14 0.02	Sensitivity 94.1% Specificity 100%	28 RT-19 TN-9
Matsusue et al.[53]	RT TN *P*-value	1.87 ± 0.39 1.11 ± 0.66 >0.05	1.56 ± 0.82 1.16 ± 0.91 >0.05	- - -	Sensitivity 90% Specificity 66.7%	15 TN-5 RT-10
Huang et al.[137]	RT TN *P*-value	1.72 ± 1.10 1.34 ± 0.48 .56	1.32 ± 1.25 1.18 ± 0.37 .46	- - -	Sensitivity 36% Specificity 55%	26 (33 lesions) TN-10* RT-23*
Elias et al.[139]	RT TN *P*-value	2.23 ± 0.78 1.84 ± 0.58 .2441	2.81 ± 0.82 1.39 ± 0.46 .0004	0.85 ± 0.40 1.36 ± 0.33 0.0033	Cho/NAA: Sensitivity 86% Specificity 90% NAA/Cr: Sensitivity 93% Specificity 70%	25 TN-10 RT-15
Other features						
	Parameter	**RT**	**TN**	***P*-value**		
Traber et al.[140]	Cho peak	>50%	<50%	-	Sensitivity 72% Specificity 82%	43
Prat et al.[65]	NAA/Cho	<0.7	>0.7	-	PPV: 100% NPV: 100%	9 TN-2, RT-7
Kamada et al.[95]	Lac/Cr Cho/Cr	1.65 ± 0.51 3.07 ± 0.23	8.55 ± 4.97 2.07 ± 0.72	<0.05 <0.05	Accuracy: 100% (Lac/Cho cutoff =1)	11 TN-5 RT-6

Abbreviations: Cho, choline; Cr, creatine; Lac, lactate; NPV, negative predictive value; PPV, positive predictive value; SD, stable disease.
*count indicates number of lesions.

lead to incorrect interpretation based on elevated lipid and lactate levels.

MRS has low spatial resolution and SNR. Although 3-dimensional MRS imaging may address this problem, to date, no 3-dimensional MRS study has conclusively demonstrated that this approach can reliably differentiate tumor recurrence from treatment necrosis. Another major limitation of MRS is the low reproducibility of the measurements. MRS requires a large number of acquisitions to achieve sufficient SNR because of the low metabolite concentrations. This results in long scan times, which in turn, result in considerable degradation of the average metabolite spectrum because of subject movement and physiological motion. Other factors that cause variability in MRS measurements include low SNR, acquisition variability, biological variability, and inaccurate voxel relocalization while spectrum averaging. The 2 most widely used

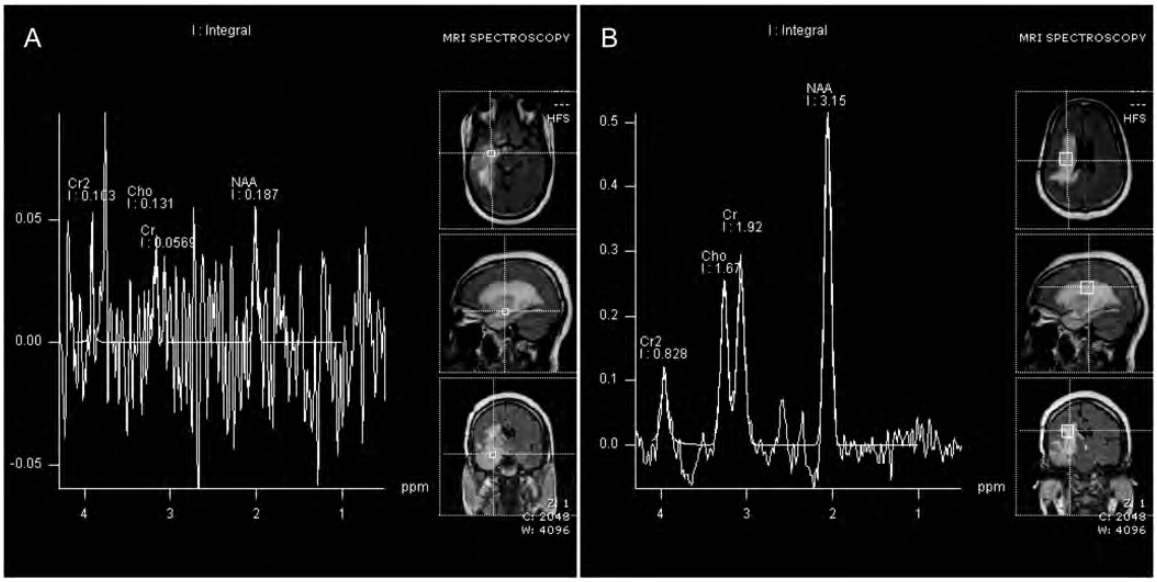

Fig. 3. MR spectroscopic imaging of patient shown in Fig. 1A with glioblastoma in temporal lobe treated with surgical resection. (A) Metabolite spectra corresponding to voxels selected inside the lesion. (B) Metabolite spectra corresponding to voxels selected inside the peri-lesional brain tissue. The lack of elevated choline (Cho) peak inside the lesion suggested treatment necrosis; however, histopathological verification proved it to be tumor recurrence.

pulse sequences for MRS are point-resolved excitation spin-echo sequence and the stimulated echo acquisition mode (STEAM) technique. Point-resolved excitation spin-echo sequence acquisitions are faster and have better SNR than STEAM. However, STEAM provides better baseline spectral measures for the metabolites. Other factors that limit the clinical use of MRS are long scan times, high cost, and no insurance coverage.[102] Similar to diffusion and perfusion imaging, MRS also shows significant variability in metabolite ratios across studies, making universal interpretations difficult. Figure 3 shows a patient with glioblastoma in the right temporal lobe who underwent surgical resection and developed a new contrast-enhancing lesion on follow-up. MRS inside the lesion (Fig. 3A) showed a lack of elevated choline peak, with normal spectra observed outside the lesion (Fig. 3B). This suggested a case of treatment necrosis; however, pathological verification proved to be tumor recurrence. The low levels of choline may be attributable to a mixture of tissue necrosis and recurrence inside the lesion.

Nuclear Medicine Imaging

Nuclear medicine uses weakly radioactive medicinal compounds known as radiopharmaceuticals to image the physiological properties of organs. The rationale for using nuclear medicine to differentiate between treatment necrosis and tumor recurrence is that the increased metabolism of an actively growing recurrent tumor will result in higher tracer uptake, compared with lesions resulting from treatment necrosis. There are 2 types of methods used for metabolic imaging of intracranial lesions: positron emission tomography (PET) and single photon emission CT (SPECT).

PET

PET produces 3-dimensional images of regional metabolic activity in a tissue based on the extent of radiotracer uptake. Fludeoxyglucose (FDG), a commonly used analogue of glucose, has been reported to be capable of distinguishing treatment necrosis from tumor recurrence with sensitivity and specificity in the ranges of 65%–81% and 40%–94%, respectively[54,63,103–108] (Table 5). However, there are some features of FDG that limit its use: (1) FDG uptake in normal cortex is variable and may make it difficult to distinguish tumor from surrounding normal gray matter and (2) low-grade tumors appear to be metabolically similar to their surrounding normal tissues, thus hindering the detection and accurate delineation of observed lesions.

Progressing tumors exhibit increased amino acid transport, and therefore, amino acid analogs, such as 3,4-dihydroxy-6–^{18}F-fluoro-L-phenylalanine (^{18}F-FDOPA), O-2-^{18}F-fluoroethyl-L-tyrosine (^{18}F–FET), and L-methyl-^{11}C-methionine (^{11}C-MET) have also been explored as potential tracers for differentiating between treatment necrosis and tumor recurrence[109,110] (Table 5). Amino acid analogs may perform better than FDG, because amino acids exhibit lower uptake in the normal cortex than does glucose, which would result in better contrast than FDG and, thus, more accurate detection of growing tumors. ^{11}C-MET has also been reported to be superior to FDG for detecting tumor recurrence and accurately determining a tumor's invasion into normal tissue for planning subsequent radiation therapy.[111–113]

Table 5. Accuracy of PET in distinguishing between treatment necrosis (TN) and recurrent tumor (RT) using different tracer types

Reference	Tracer	Specificity (%)	Sensitivity (%)	Number of patients
Gomez-Rio et al.[107]	^{18}F-FDG	95	78	76(RT-55, TN-21)
Ozsunar et al.[63]	^{18}F-FDG	90	81	26(RT-14, TN-12)
Di Chiro et al.[104]	^{18}F-FDG	100	100	95(RT-85, TN-10)
Valk et al.[105]	^{18}F-FDG	88.24	80.95	38(RT-17, TN-21)
Ricci et al.[103]	^{18}F-FDG	22	86	31(RT-22, TN-9)
Kim et al.[106]	^{18}F-FDG	94	80	33(RT-15, TN-18)
Janus et al.[108]	^{18}F-FDG	62.5	83.33	20(RT-12, TN-8)
Dong-Li et al.	^{18}F-FDG -PET/CT	88.9	50	36(RT-28, TN-8)
Popperl et al.[141]	^{18}F-FET	100	100	53(RT-42, TN-11)
Rachinger et al.[142]	^{18}F-FET	100	92.9	45(RT-31, TN-14)
Chen et al.[114]	^{18}F-FDOPA	86	98	81(RT-28, TN-15, SD-27, PT-11)
Terakawa et al.[143]	^{11}C-MET	75	75	77(88 scans: RT-40, TN-48)*
Tsuyuguchi et al.[144]	^{11}C-MET	60	100	11(RT-6, TN-5)
Kim et al.[54]	^{11}C-MET	100	75	10(RT-4, TN-6)
Laere et al.[112]	^{11}C-MET	70	75	22(RT-18, TN-4)
Dong-Li et al.[111]	^{11}C-MET-PET/CT	83.3	88.5	36(RT-28, TN-8)

Abbreviations: PT, primary tumor; SD, stable disease.
*Multiple scans performed for each patient and, therefore, the RT and RN count represents number of scans.

However, the accumulation of ^{11}C-MET in necrotic tissues and the relatively short half-life of ^{11}C limit the use of ^{11}C-MET. Therefore, ^{18}F aromatic amino acid analogs, such as ^{18}F-FDOPA, with longer half-lives and lower normal gray matter tracer uptake have been investigated and reported to be superior to ^{18}F-FDG for detecting low-grade tumors and evaluating brain tumor recurrence, differentiating among tumor grades, and distinguishing tumor recurrence from treatment necrosis.[114]

There are some features of PET imaging that limit its use for differentiating between tumor recurrence and treatment necrosis: (1) some conditions (e.g. epilepticus) can increase glucose metabolism in areas of the brain and may be misinterpreted as a progressing tumor, (2) radiation injury can trigger repair mechanisms that increase glucose metabolism in the brain and give the false impression of tumor recurrence, (3) PET images have generally low spatial resolution (~5 mm) that limits their sensitivity in early detection of recurrence, and (4) there are risks to patients associated with exposure to ionizing gamma radiation. Most of the current commercially available scanners have the ability to perform PET in combination with CT. The combination of PET/CT helps with (1) better lesion localization by combining anatomical and functional information, (2) greater distinction between physiological (normal brain tissue) and pathological (tumor) radiotracer uptake that improves the sensitivity of detection using PET, and (3) improving the efficiency of the attenuation correction process (correcting for absorption by interposed tissue) in PET that reduces the scan time from approximately 60 min to 30–45 min. Although PET/CT is more expensive than routine imaging (MRI or CT), it is covered by insurance and, thus, has potential clinical use. The only drawback in using this hybrid scan is that it involves patient exposure to ionizing radiation. However, significant attempts are being made to create combined PET/MR systems that would further improve the resolution and reduce the risk of exposure to ionizing radiation.

SPECT

SPECT is similar to conventional planar nuclear medicine imaging but provides additional 3-dimensional information about an organ by imaging from multiple angles with use of gamma rays. Several radiotracers such as Thallium-201 (^{201}Tl), ^{99m}Tc-sestamibi, Iodine-123-a-methyl tyrosine (^{123}I-IMT), ^{999m}Tc-glucoheptonate, and ^{99m}Tc-tetrofosmin have been used with SPECT for imaging brain lesions. ^{201}Tl is not incorporated into healthy brain tissue and has been reported to be superior to more powerfully differentiate treatment necrosis from tumor recurrence, compared with conventional structural imaging;[115,116] however, there is some variability in the power of this method, which was recently reported to have sensitivity ranging from 43% to 100% and specificity ranging from 25% to 100% (Table 6).[117] In addition, ^{201}Tl SPECT has low spatial resolution and requires relatively large radiation doses.

To overcome these limitations, several ^{99m}Technetium-based tracers have been developed that have higher photon flux, thereby providing better spatial resolution and requiring lower radiation doses than ^{201}Tl (Table 6).[118–124] However, tracer uptake in the normal tissues of the choroid plexus and pituitary gland has limited their clinical use. The sensitivity of these tracers is also low when attempting to detect tumor recurrence in the posterior fossa region. P-glycoproteins may

Table 6. Accuracy of SPECT in distinguishing between recurrent tumor (RT) and treatment necrosis (TN) using different tracer types.

Reference	Tracer	Specificity (%)	Sensitivity (%)	Number of patients
Gomez-Rio et al.[107]	^{201}Tl	86	93	76 (RT-55, TN-21)
Tie et al.[116]	^{201}Tl	100	84	19 (21 scans: RT-17, TN-4)*
Kline et al.[145]	^{201}Tl	63	94	33 (42 scans: RT-34, TN-8)*
Yamamoto et al.[146]	^{201}Tl	50	100	21 (RT-15, TN-6)
Mountz et al.[122]	^{99m}Tc-sestamibi	100	100	20
Lamy-Lhullier[118]	^{99m}Tc-sestamibi	85	73	22 (RT-15, TN-7)
Henze et al.[119]	^{99m}Tc-sestamibi	75	53	16 (25 lesions, RT-17, TN-8)**
Palumbo et al.[120]	^{99m}Tc-sestamibi	100	91	30 (RT-20, TN-10)
Le Jeune et al.[121]	^{99m}Tc-sestamibi	91.5	90	81 (201 scans: RT-113, TN-88)*
Henze et al.[119]	^{123}I-IMT	100	94	16 (25 lesions, RT-17, TN-8)**
Samnick et al.[126]	^{123}I-IMT	100	94	78 (RT-68, TN-10)
Kuwert et al.[127]	^{123}I-IMT	100	78	27 (31 scans: RT-23, TN-8)*
Alexiou et al.[124]	^{99m}Tc-tetrofosmin	100	100	11 (RT-8, TN-3)
Barai et al.[125]	^{99m}Tc-glucoheptonate	100	100	20 (RT-17, TN-3)

*Multiple scans per performed for each patient and therefore, the RT and TN count represents number of scans.
**Multiple lesions in patients. The differentiation was done on each lesion.

also remove these tracers from tumor cells, thereby reducing their sensitivity to detect growing tumors. ^{99m}Tc-glucoheptonate is another technetium-based tracer that has been reported to exhibit diagnostic power similar to that of ^{99m}Tc-tetrofosmin for detecting tumor recurrence[123,125] and has the additional advantages of no uptake in the choroid plexus and not being targeted by P-glycoproteins. Barai et al.[125] compared the performance of ^{201}Tl and ^{99m}Tc-glucoheptonate, reporting that both tracers accurately identified lesions resulting from treatment necrosis; however, ^{99m}Tc-glucoheptonate performed better on tumor recurrence lesions and provided important information about a tumor's margin, its extent of infiltration, and the amount of necrosis inside a lesion. Another commonly used tracer is an artificial amino acid, ^{123}I-IMT, which exhibits high uptake in tumors but is not incorporated into cellular proteins, meaning that its accumulation reflects only the amino acid transport. Studies have reported high accuracy of ^{123}I-IMT both for grading tumors and differentiating tumor recurrence from treatment necrosis;[119,126,127] however, low availability and low sensitivity to detect small lesions currently limit the use of ^{123}I-IMT.

SPECT has poor spatial resolution (~7 mm) and low SNR. The localization of radiotracer uptake is also difficult in SPECT, because its low spatial resolution does not allow accurate registration of the functional images with the anatomical images (from MRI or CT). Similar to PET/CT, the combination of SPECT/CT has also been proposed to overcome some of the limitations of SPECT, such as poor spatial resolution, low SNR, and poor localization of radiotracer accumulations. However, SPECT/CT never attained the popularity of PET/CT. This is because, unlike PET/CT, the addition of CT does not increase the speed of SPECT. Furthermore, the relative increase in cost of adding CT to SPECT scanners is much higher than adding CT to PET.

Multimodality Functional Imaging for Brain Tumor Follow-Up

Functional imaging provides important physiological information that complements the anatomical information obtained through structural imaging and can be used to differentiate between tumor recurrence and treatment necrosis. However, the majority of studies thus far have considered imaging modalities independently or compared the performance of different tracers. Although functional imaging is capable of differentiating tumor recurrence from treatment necrosis, its reliability decreases when cases present with lesions resulting from a combination of recurrence and treatment necrosis. The relative abundances of tissue necrosis and growing tumor inside a lesion may skew the values of some quantitative parameters estimated from functional images and, thus, mislead the interpretation of a lesion as purely treatment necrosis, purely tumor recurrence, or even normal brain tissue.

To overcome these limitations, the combination of multiple imaging modalities has been proposed to be more powerful than a single modality approach for differentiating between treatment necrosis and tumor recurrence. Floeth et al.[128] reported that the accuracy to detect brain tumors increased from 68% to 97% when structural MRI was used in conjunction with FET-PET and MRS. Nakajima et al.[64] and Zeng et al.[39] also reported substantially improved discriminatory power when MRS was used in conjunction with DWI. Prat et al.[65] suggested that MRS and MR perfusion were the most promising imaging methods for detecting tumor recurrence, because both have good spatial resolution. They also discouraged the exclusive use of a single modality to observe patients because it decreased the positive predictive value of detecting tumor recurrence. In a recent study, Matsusue et al.[53] implemented

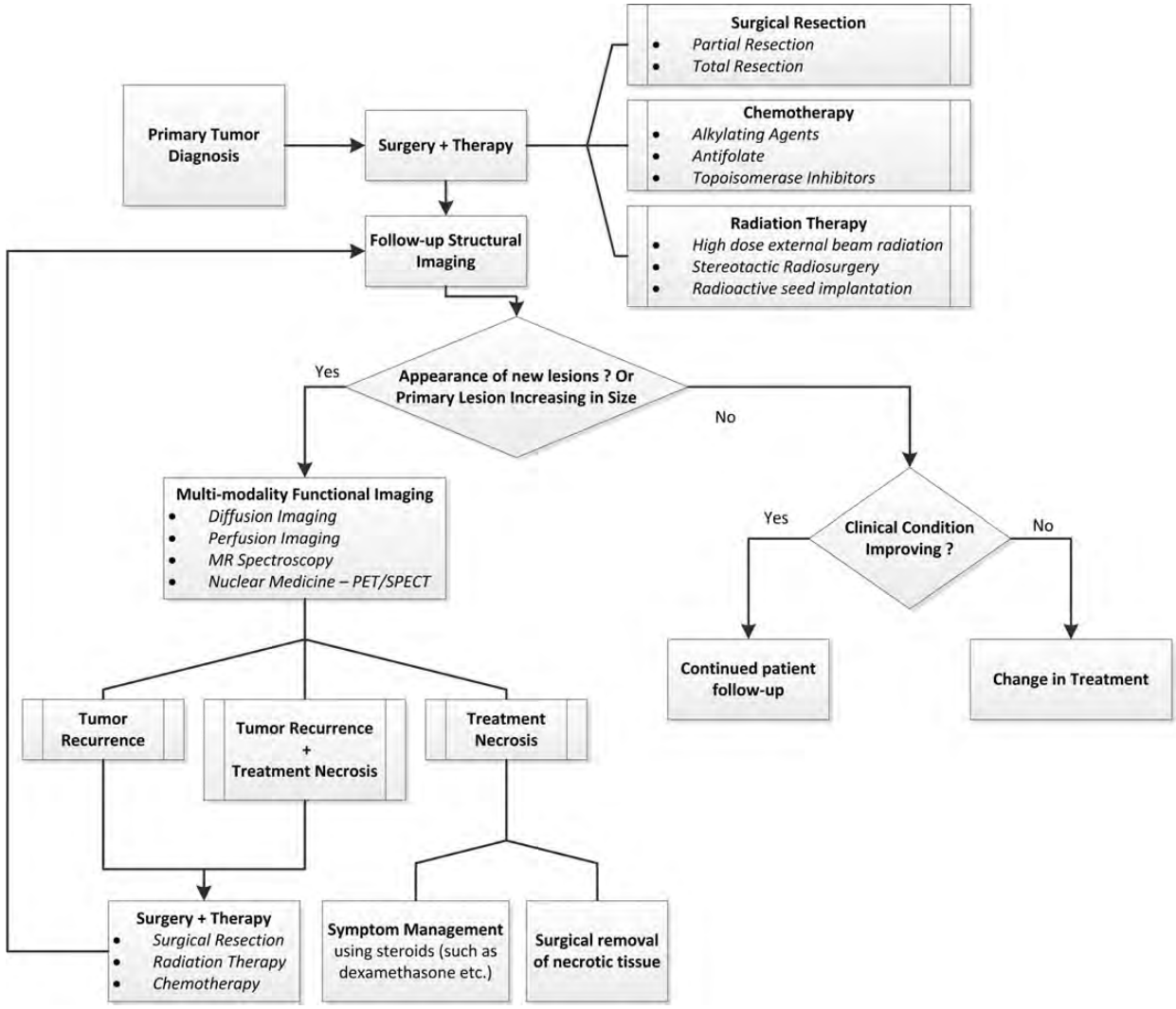

Fig. 4. Flowchart illustrating the proposed flexible treatment algorithm that combines multiple functional imaging techniques with structural imaging for treatment of patients with brain tumor.

a multiparametric diffusion imaging, perfusion imaging, and MRS system and reported accuracy that was significantly better than that of any single modality for differentiating between tumor recurrence and treatment necrosis. Rock et al.[32] also reported that combining DWI and PET provided much more reliable differentiation between tumor recurrence and treatment necrosis. However, the use of multiple functional imaging methods is costly, extremely time-consuming, unlikely to be covered by most insurance plans at this time, and thus, impractical in the current clinical setting.

We propose a flexible treatment plan (Fig. 4) that combines multiple functional and structural imaging methods to provide valuable physiological information about a lesion and to reliably differentiate between treatment necrosis and tumor recurrence. On the basis of the findings reported in literature, the following cues may indicate tumor recurrence:

Diffusion Imaging (DTI/DWI)	Lower ADC values and higher FA values
Perfusion Imaging	Higher rCBV and rPH; and lower PSR values
MR Spectroscopy	Higher Cho/Cr and Cho/NAA ratios
Nuclear medicine (PET/SPECT)	Hyper-metabolic regions

In the case of a new contrast-enhancing lesion observed on a patient's follow-up images, the physiological information from functional imaging modalities can be combined with information regarding patient demographic characteristics, therapeutic history, and the primary tumor type to help determine the etiology of the lesion and plan treatment accordingly. It is also possible for residual tumor to recur at the resection site, in which case the resection may show increased size and/

or contrast. Further investigation with functional imaging methods would help determine whether the enhancement at the resection site is a consequence of treatment necrosis or tumor recurrence. In addition, when the lesion at a resection site is shrinking or stable, a patient's clinical condition may be the most important information for determining a treatment's effectiveness. Symptom improvement indicates effective treatment, and patients can continue routine follow-up imaging until full recovery; in contrast, when a patient's condition is deteriorating, a change in treatment is needed.

Quantitative Morphological Analysis of Image Features

Although functional imaging methods show promise for differentiating tumor recurrence from treatment necrosis, the clinical use of most functional modalities is limited by acquisition variability, unreliable predictions, low clinical availability, high operational costs, and low insurance coverage. Moreover, most studies to evaluate functional imaging have had small sample size and lack of unambiguous pathological validation of the lesions considered. Therefore, functional imaging needs further evaluation to establish its reliability and robustness for differentiating between the 2 outcome types.

The current standard of care for observing patients with brain tumor is structural MRI, often with the addition of DWI to provide additional functional information. However, tumor recurrence and treatment necrosis exhibit grossly similar characteristics (such as edema, necrosis, and mass effect) on such images. Radiologic images are currently interpreted through qualitative visual inspection, which limits the power for differentiating tumor recurrence from treatment necrosis. However, because the physiology underlying the development of treatment necrosis and tumor recurrence is different, it is reasonable to expect that there may be some fine-grained differences between these 2 outcomes that might not be obvious by visual inspection. Structural imaging features have been identified that hold promise for differentiating tumor recurrence from treatment necrosis.[1,2] However, previous investigations have often used image characteristics that were subjectively assessed and qualitatively defined and, therefore, potentially have interobserver variability. Moreover, qualitatively defined features cannot capture the fine differences that may separate images that are highly similar in overall appearance. Such drawbacks have resulted in limited success reported by such studies in differentiating between the 2 outcome types.

Quantitative MRI research in this domain to date has mainly been very basic investigation of low-level image features, such as sampling of image intensities in different regions of the lesion, which has limited success in distinguishing between the 2 treatment outcome types.[129,130] Advanced approaches involving morphometric analyses of features observed on structural and functional imaging has been mostly unexplored for its potential to discriminate between treatment necrosis and tumor recurrence. Such an approach has been extensively used for noninvasive tumor grading, brain tumor classification, and predicting patient prognosis.[131–136] A quantitative approach could address most of the limitations of the current methods of image interpretation and provide additional information about lesions to physicians to better discriminate between tumor recurrence and treatment necrosis.

Conclusion

Patients with brain tumor often develop new areas of contrast enhancement on routine follow-up imaging which can be the result of treatment necrosis, tumor recurrence, or a combination of the 2 outcomes. Identifying the etiology of a lesion is of vital importance in neuro-oncology for both diagnosis and treatment planning purposes. Structural imaging is widely used to observe patients with brain tumor but is generally thought to be inadequate for reliably distinguishing between treatment necrosis and tumor recurrence, because both lesion types appear to be grossly similar on imaging. The gold standard for differentiating between tumor recurrence and treatment necrosis is biopsy, which is expensive and involves risks associated with surgery. Therefore, there is an increased interest in neuro-oncology in the development of noninvasive methods that can differentiate between the 2 lesion types. A noninvasive method of differentiating between the 2 outcome types will help prevent unnecessary interventions in patients, reducing health care costs and improving patient survival and quality of life.

Functional imaging methods provide important physiological information about a lesion and can be helpful when attempting to differentiate between tumor recurrence and treatment necrosis. The majority of effort thus far has focused on investigating the efficacy of single functional imaging modalities; these studies have generally reported lower level evidence resulting from small sample sizes and lack of histopathological verification of lesion type. Furthermore, functional imaging has been reported to be inaccurate in classifying cases in which a lesion consists of a mixture of treatment necrosis and tumor recurrence. In such scenarios, the use of multiple functional imaging modalities would be recommended because the different modalities would each provide unique information about the physiology of the lesion. In addition, the use of multiple imaging methods is expected to have reduced chance of lesion misinterpretation relative to single imaging modality.

Although functional imaging methods have potential in differentiating between tumor recurrence and treatment necrosis, the clinical use of many functional modalities is currently limited by low availability of scanners, high operation costs, and lack of insurance coverage. Because reliable diagnosis may often require use of multiple functional imaging methods, these limitations make the use of many functional imaging techniques impractical in clinical settings. Although the gross appearances of treatment necrosis and tumor

recurrence are similar on routine imaging, fine-grained differences between the 2 outcome types have not been investigated in much detail. Quantitative approaches involving morphometric analysis of image features observed on routine imaging hold promise in differentiating between tumor recurrence and treatment necrosis, addressing most of the limitations in earlier studies.

Conflict of interest statement. None declared.

References

1. Kumar AJ, Leeds NE, Fuller GN, et al. Malignant gliomas: MR imaging spectrum of radiation therapy- and chemotherapy-induced necrosis of the brain after treatment. *Radiology*. 2000;217(2):377–384.
2. Mullins ME, Barest GD, Schaefer PW, et al. Radiation necrosis versus glioma recurrence: conventional MR imaging clues to diagnosis. *AJNR Am J Neuroradiol*. 2005;26(8):1967–1972.
3. Curnes J, Laster D, Ball M, et al. MRI of radiation injury to the brain. *Am J Roentgenol*. 1986;147(1):119–124.
4. Brismar J, Roberson GH, Davis KR. Radiation necrosis of the brain. Neuroradiological considerations with computed tomography. *Neuroradiology*. 1976;12(2):109–113.
5. Mikhael M. Radiation necrosis of the brain: correlation between computed tomography, pathology, and dose distribution. *J comput Assist Tomogr*. 1978;2(1):71–80.
6. Dellen Jv, Danzinger A. Failure of computerized tomography to differentiate between radiation necrosis and cerebral tumor. *S Afr Med J*. 1978;53(5):171–172.
7. Kingsley D, Kendall B. CT of the adverse effects of therapeutic radiation of the central nervous system. *AJNR Am J Neuroradiol*. 1981;2(5):453–460.
8. Leibel S, Sheline G. Tolerance of the brain and spinal cord to conventional irradiation. *Radiation Injury to the Nervous system*. Gutin P, Leibel S, Sheline G (Eds), Raven Press, New York, 1991, p. 239.
9. Wong CS, Van der Kogel AJ. Mechanisms of radiation injury to the central nervous system: implications for neuroprotection. *Molecular interventions*. 2004;4(5):273.
10. Lyubimova N, Hopewell JW. Experimental evidence to support the hypothesis that damage to vascular endothelium plays the primary role in the development of late radiation-induced CNS injury. *Br J Radiol*. 2004;77(918):488–492.
11. Schultheiss TE, Stephens LC. Permanent radiation myelopathy. *British Journal of Radiology*. 1992;65(777):737–753.
12. Brandsma D, Stalpers L, Taal W, et al. Clinical features, mechanisms, and management of pseudoprogression in malignant gliomas. *The Lancet Oncology*. 2008;9(5):453–461.
13. Marks JE, Baglan RJ, Prassad SC, et al. Cerebral radionecrosis: incidence and risk in relation to dose, time, fractionation and volume. *International Journal of Radiation Oncology* Biology* Physics*. 1981;7(2):243–252.
14. Sheline GE, Wara WM, Smith V. Therapeutic irradiation and brain injury. *International Journal of Radiation Oncology* Biology* Physics*. 1980;6(9):1215–1228.
15. Leibel SA, Sheline GE. Radiation therapy for neoplasms of the brain. *Journal of Neurosurgery*. 1987;66(1):1–22.
16. Chamberlain MC, Glantz MJ, Chalmers L, et al. Early necrosis following concurrent Temodar and radiotherapy in patients with glioblastoma. *Journal of Neuro-oncology*. 2007;82(1):81–83.
17. Byme T. Imaging of gliomas. *Semin Oncol*. 1994;21:162–171.
18. Leeds N, Jackson E. Current imaging techniques for the evaluation of brain neoplasms. *Curr Opin Oncol*. 1994;6:254–261.
19. Chan Y-l, Leung S-f, King AD, et al. Late radiation injury to the temporal lobes: morphologic evaluation at MR imaging1. *Radiology*. 1999;213(3):800–807.
20. Brennan KM, Roos MS, Budinger TF, et al. A study of radiation necrosis and edema in the canine brain using positron emission tomography and magnetic resonance imaging. *Radiation Research*. 1993;134(1):43–53.
21. Frytak S, Earnest F, O'Neill B, et al. Magnetic resonance imaging for neurotoxicity in long-term survivors of carcinoma. *Mayo Clin., Proc*. 1985;60(12):803–812.
22. Tsuruda J, Kortman K, Bradley W, et al. Radiation effects on cerebral white matter: MR evaluation. *Am J Roentgenol*. 1987;149(1):165–171.
23. Kato T, Yutaka S, Tada M, et al. Long term evaluation of Radiation-induced brain damage by serial magnetic resonance imaging. *Neurologia Medico-Chirurgica*. 1996;36(12):870–876.
24. Moody D, Bell M, Challa V. Features of the cerebral vascular pattern that predict vulnerability to perfusion or oxygenation deficiency: an anatomic study. *Am J Neuroradiol*. 1990;11(3):431–439.
25. Macdonald DR, Cascino TL, Schold SC, et al. Response criteria for phase II studies of supratentorial malignant glioma. *Journal of Clinical Oncology*. 1990;8(7):1277–1280.
26. Wen PY, Macdonald DR, Reardon DA, et al. Updated response assessment criteria for high-grade gliomas: response assessment in neuro-oncology working group. *Journal of Clinical Oncology*. 2010;28(11):1963–1972.
27. Sorensen AG, Batchelor TT, Wen PY, et al. Response criteria for glioma. *Nat Clin Prac Oncol*. 2008;5(11):634–644.
28. Jain R, Scarpace L, Ellika S, et al. Imaging response criteria for recurrent gliomas treated with bevacizumab: Role of diffusion weighted imaging as an imaging biomarker. *Journal of Neuro-Oncology*. 2010;96(3):423–431.
29. Zuniga R, Torcuator R, Jain R, et al. Efficacy, safety and patterns of response and recurrence in patients with recurrent high-grade gliomas treated with bevacizumab plus irinotecan. *Journal of Neuro-Oncology*. 2009;91(3):329–336.
30. Henson JW, Ulmer S, Harris GJ. Brain tumor imaging in clinical trials. *Am J Neuroradiol*. 2008;29(3):419–424.
31. Hein PA, Eskey CJ, Dunn JF, et al. Diffusion-weighted imaging in the follow-up of treated high-grade gliomas: tumor recurrence versus radiation injury. *AJNR Am J Neuroradiol*. 2004;25(2):201–209.
32. Rock JP, Scarpace L, Hearshen D, et al. Associations among magnetic resonance spectroscopy, apparent diffusion coefficients, and image-guided histopathology with special attention to radiation necrosis. *Neurosurgery*. 2004;54(5):1111.
33. Lam WWM, Poon WS, Metreweli C. Diffusion MR imaging in glioma: does it have any role in the pre-operation determination of grading of glioma? *Clinical Radiology*. 2002;57(3):219–225.
34. Sugahara T, Korogi Y, Kochi M, et al. Usefulness of diffusion-weighted MRI with echo-planar technique in the evaluation of cellularity in gliomas. *Journal of Magnetic Resonance Imaging*. 1999;9(1):53–60.

35. Sinha S, Bastin ME, Whittle IR, et al. Diffusion tensor MR imaging of high-grade cerebral gliomas. *Am J Neuroradiol*. 2002;23(4):520–527.
36. Provenzale JM, McGraw P, Mhatre P, et al. Peritumoral brain regions in gliomas and meningiomas: investigation with isotropic diffusion-weighted MR Imaging and diffusion-tensor MR imaging1. *Radiology*. 2004;232(2):451–460.
37. Xu J-L, Li Y-L, Lian J-M, et al. Distinction between postoperative recurrent glioma and radiation injury using MR diffusion tensor imaging. *Neuroradiology*. 2010;52(12):1193–1199.
38. Asao C, Korogi Y, Kitajima M, et al. Diffusion-weighted imaging of radiation-induced brain injury for differentiation from tumor recurrence. *AJNR Am J Neuroradiol*. 2005;26(6):1455–1460.
39. Zeng Q-S, Li C-F, Liu H, et al. Distinction between recurrent glioma and radiation injury using magnetic resonance spectroscopy in combination with diffusion-weighted imaging. *International Journal of Radiation Oncology*Biology*Physics*. 2007;68(1):151–158.
40. Al Sayyari A, Buckley R, McHenery C, et al. Distinguishing recurrent primary brain tumor from radiation injury: a preliminary study using a susceptibility-weighted MR imaging-guided apparent diffusion coefficient analysis strategy. *AJNR Am J Neuroradiol*. 2010;31(6):1049–1054.
41. Biousse V, Newman NJ, Hunter SB, et al. Diffusion weighted imaging in radiation necrosis. *Journal of Neurology, Neurosurgery & Psychiatry*. 2003;74(3):382–384.
42. Sundgren PC, Fan X, Weybright P, et al. Differentiation of recurrent brain tumor versus radiation injury using diffusion tensor imaging in patients with new contrast-enhancing lesions. *Magnetic Resonance Imaging*. 2006;24(9):1131–1142.
43. Lu S, Ahn D, Johnson G, et al. Diffusion-tensor MR imaging of intracranial neoplasia and associated peritumoral edema: introduction of the tumor infiltration index1. *Radiology*. 2004;232(1):221–228.
44. Price SJ, Peña A, Burnet NG, et al. Tissue signature characterisation of diffusion tensor abnormalities in cerebral gliomas. *European Radiology*. 2004;14(10):1909–1917.
45. Inoue T, Ogasawara K, Beppu T, et al. Diffusion tensor imaging for preoperative evaluation of tumor grade in gliomas. *Clinical Neurology and Neurosurgery*. 2005;107(3):174–180.
46. Kitahara S, Nakasu S, Murata K, et al. Evaluation of treatment-induced cerebral white matter injury by using diffusion-tensor MR imaging: initial experience. *AJNR Am J Neuroradiol*. 2005;26(9):2200–2206.
47. Kashimura H, Inoue T, Beppu T, et al. Diffusion tensor imaging for differentiation of recurrent brain tumor and radiation necrosis after radiotherapy–Three case reports. *Clinical Neurology and Neurosurgery*. 2007;109(1):106–110.
48. Witwer BP, Moftakhar R, Hasan KM, et al. Diffusion tensor imaging of white matter tracts in patients with cerebral neoplasm. *J Neurosurg* 2002;97(3):568–575.
49. Melhem ER, Mori S, Mukundan G, et al. Diffusion tensor MR imaging of the brain and white matter tractography. *American Journal of Roentgenology*. 2002;178(1):3–16.
50. Koh DM, Amoozadeh Y, Blackledge M, et al. Diffusion-weighted MR Imaging: Applications in the Body: *Medical Radiology*, Springer, Heidelberg; (2010).
51. Folsted Kallehauge J, Tanderup K, Muren LP, et al. Apparent Diffusion Coefficient (ADC) as a quantitative parameter in diffusion weighted MR imaging in gynecologic cancer: Dependence on b-values used. *Acta Oncologica (Stockholm)(online)*. 2010;49(7):1017–1022.
52. Yoshiura T, Wu O, Zaheer A, et al. Highly diffusion-sensitized MRI of brain: Dissociation of gray and white matter. *Magnetic resonance in medicine*. 2001;45(5):734–740.
53. Matsusue E, Fink J, Rockhill J, et al. Distinction between glioma progression and post-radiation change by combined physiologic MR imaging. *Neuroradiology*. 2010;52(4):297–306.
54. Kim YH, Oh SW, Lim YJ, et al. Differentiating radiation necrosis from tumor recurrence in high-grade gliomas: Assessing the efficacy of 18F-FDG PET, 11C-methionine PET and perfusion MRI. *Clinical Neurology and Neurosurgery*. 2010;112(9):758–765.
55. Barajas RF, Chang JS, Segal MR, et al. Differentiation of recurrent glioblastoma multiforme from radiation necrosis after external beam radiation therapy with dynamic susceptibility-weighted contrast-enhanced perfusion MR imaging1. *Radiology*. 2009;253(2):486–496.
56. Barajas RF, Chang JS, Sneed PK, et al. Distinguishing recurrent intra-axial metastatic tumor from radiation necrosis following gamma knife radiosurgery using dynamic susceptibility-weighted contrast-enhanced perfusion MR imaging. *AJNR Am J Neuroradiol*. 2009;30(2):367–372.
57. Mitsuya K, Nakasu Y, Horiguchi S, et al. Perfusion weighted magnetic resonance imaging to distinguish the recurrence of metastatic brain tumors from radiation necrosis after stereotactic radiosurgery. *Journal of Neuro-Oncology*. 2010;99(1):81–88.
58. Sugahara T, Korogi Y, Tomiguchi S, et al. Posttherapeutic intraaxial brain tumor: the value of perfusion-sensitive contrast-enhanced MR imaging for differentiating tumor recurrence from nonneoplastic contrast-enhancing tissue. *AJNR Am J Neuroradiol*. 2000;21(5):901–909.
59. Hazle JD, Jackson EF, Schomer DF, et al. Dynamic imaging of intracranial lesions using fast spin-echo imaging: Differentiation of brain tumors and treatment effects. *Journal of Magnetic Resonance Imaging*. 1997;7(6):1084–1093.
60. Covarrubias DJ, Rosen BR, Lev MH. Dynamic magnetic resonance perfusion imaging of brain tumors. *The Oncologist*. 2004;9(5):528–537.
61. Lupo JM, Cha S, Chang SM, et al. Dynamic susceptibility-weighted perfusion imaging of high-grade gliomas: characterization of spatial heterogeneity. *AJNR Am J Neuroradiol*. 2005;26(6):1446–1454.
62. Cha S, Lu S, Johnson G, Knopp EA. Dynamic susceptibility contrast MR imaging: Correlation of signal intensity changes with cerebral blood volume measurements. *Journal of Magnetic Resonance Imaging*. 2000;11(2):114–119.
63. Ozsunar Y, Mullins ME, Kwong K, et al. Glioma recurrence versus radiation necrosis?: A pilot comparison of arterial spin-labeled, dynamic susceptibility contrast enhanced MRI, and FDG-PET imaging. *Academic Radiology*. 2010;17(3):282–290.
64. Nakajima T, Kumabe T, Kanamori M, et al. Differential diagnosis between radiation necrosis and glioma progression using sequential proton magnetic resonance spectroscopy and methionine positron emission tomography. *Neurologia Medico-Chirurgica*. 2009;49(9):394–401.
65. Prat R, Galeano I, Lucas A, et al. Relative value of magnetic resonance spectroscopy, magnetic resonance perfusion, and 2-(18F) fluoro-2-deoxy-D-glucose positron emission tomography for detection of recurrence or grade increase in gliomas. *Journal of Clinical Neuroscience*. 2010;17(1):50–53.
66. Kamiryo T, Lopes MB, Kassell NF, et al. Radiosurgery-induced microvascular alterations precede necrosis of the brain neuropil. *Neurosurgery*. 2001;49(2):409–415.

67. Hou L, Yang Y, Mattay VS, et al. Optimization of fast acquisition methods for whole-brain relative cerebral blood volume (rCBV) mapping with susceptibility contrast agents. *Journal of Magnetic Resonance Imaging*. 1999;9(2):233–239.
68. Bisdas S, Naegele T, Ritz R, et al. Distinguishing recurrent high-grade gliomas from radiation injury: a pilot study using dynamic contrast-enhanced MR imaging. *Academic Radiology*. 2011;18(5):575–583.
69. Narang J, Jain R, Arbab AS, et al. Differentiating treatment-induced necrosis from recurrent/progressive brain tumor using nonmodel-based semiquantitative indices derived from dynamic contrast-enhanced T1-weighted MR perfusion. *Neuro-Oncology*. 2011;13(9):1037–1046.
70. Chih-Feng C, Ling-Wei H, Chun-Chung L, et al. In vivo correlation between semi-quantitative hemodynamic parameters and Ktrans derived from DCE-MRI of brain tumors. *International Journal of Imaging Systems and Technology*. 2012;22(2):132–136.
71. Buckley DL. Uncertainty in the analysis of tracer kinetics using dynamic contrast-enhanced T1-weighted MRI. *Magnetic Resonance in Medicine*. 2002;47(3):601–606.
72. Tofts PS, Brix G, Buckley DL, et al. Estimating kinetic parameters from dynamic contrast-enhanced T 1-weighted MRI of a diffusable tracer: standardized quantities and symbols. *Journal of Magnetic Resonance Imaging*. 1999;10(3):223–232.
73. Choyke PL, Dwyer AJ, Knopp MV. Functional tumor imaging with dynamic contrast-enhanced magnetic resonance imaging. *Journal of Magnetic Resonance Imaging*. 2003;17(5):509–520.
74. Evelhoch JL. Key factors in the acquisition of contrast kinetic data for oncology. *Journal of Magnetic Resonance Imaging*. 1999;10(3):254–259.
75. Taylor JS, Tofts PS, Port R, et al. MR imaging of tumor microcirculation: promise for the new millenium. *Journal of Magnetic Resonance Imaging*. 1999;10(6):903–907.
76. Jain R, Ellika SK, Scarpace L, et al. Quantitative estimation of permeability surface-area product in astroglial brain tumors using perfusion CT and correlation with histopathologic grade. *AJNR Am J Neuroradiol*. 2008;29(4):694–700.
77. Ellika SK, Jain R, Patel SC, et al. Role of perfusion CT in glioma grading and comparison with conventional MR imaging features. *AJNR Am J Neuroradiol*. 2007;28(10):1981–1987.
78. Jain R, Scarpace L, Ellika S, et al. First-pass perfusion computed tomography: initial experience in differentiating recurrent brain tumors from radiation effects and radiation necrosis. *Neurosurgery*. 2007;61(4):778.
79. Rock JP, Hearshen D, Scarpace L, et al. Correlations between magnetic resonance spectroscopy and image-guided histopathology, with special attention to radiation necrosis. *Neurosurgery*. 2002;51(4):912–920.
80. Croteau D, Scarpace L, Hearshen D, et al. Correlation between magnetic resonance spectroscopy imaging and image-guided biopsies: semiquantitative and qualitative histopathological analyses of patients with untreated glioma. *Neurosurgery*. 2001;49(4):823–829.
81. Dowling C, Bollen AW, Noworolski SM, et al. Preoperative proton MR spectroscopic imaging of brain tumors: correlation with histopathologic analysis of resection specimens. *AJNR Am J Neuroradiol*. 2001;22(4):604–612.
82. Delorme S, Weber M. Applications of MRS in the evaluation of focal malignant brain lesions. *Cancer Imaging*. 2006;6(1):95–99.
83. Doganay S, Altinok T, Alkan A, et al. The role of MRS in the differentiation of benign and malignant soft tissue and bone tumors. *European Journal of Radiology*. 2011;79(2):e33–e37.
84. Lampert PW, Davis RL. Delayed effects of radiation on the human central nervous system. Early and late delayed reactions. *Neurology*. 1964;14:912–917.
85. Schlemmer HP, Bachert P, Henze M, et al. Differentiation of radiation necrosis from tumor progression using proton magnetic resonance spectroscopy. *Neuroradiology*. 2002;44(3):216–222.
86. Schlemmer H-P, Bachert P, Herfarth KK, et al. Proton MR spectroscopic evaluation of suspicious brain lesions after stereotactic radiotherapy. *AJNR Am J Neuroradiol*. 2001;22(7):1316–1324.
87. Chong VFH, Rumpel H, Fan YF, et al. Temporal lobe changes following radiation therapy: imaging and proton MR spectroscopic findings. *European Radiology*. 2001;11(2):317–324.
88. Chong VFH, Rumpel H, Aw Y-S, et al. Temporal lobe necrosis following radiation therapy for nasopharyngeal carcinoma: 1H MR spectroscopic findings. *International Journal of Radiation Oncology, Biology, Physics*. 1999;45(3):699–705.
89. Zeng Q-S, Li C-F, Zhang K, et al. Multivoxel 3D proton MR spectroscopy in the distinction of recurrent glioma from radiation injury. *Journal of Neuro-Oncology*. 2007;84(1):63–69.
90. McKnight TR, von dem Bussche MH, Vigneron DB, et al. Histopathological validation of a three-dimensional magnetic resonance spectroscopy index as a predictor of tumor presence. *Journal of Neurosurgery*. 2002;97(4):794–802.
91. Weybright P, Sundgren PC, Maly P, et al. Differentiation between brain tumor recurrence and radiation injury using MR spectroscopy. *Am. J Roentgenol*. 2005;185(6):1471–1476.
92. Yang I, Huh NG, Smith ZA, et al. Distinguishing glioma recurrence from treatment effect after radiochemotherapy and immunotherapy. *Neurosurgery Clinics of North America*. 2010;21(1):181–186.
93. Smith EA, Carlos RC, Junck LR, et al. Developing a clinical decision model: MR spectroscopy to differentiate between recurrent tumor and radiation change in patients with new contrast-enhancing lesions. *Am J Roentgenol*. 2009;192(2):W45–52.
94. Plotkin M, Eisenacher J, Bruhn H, et al. I-IMT SPECT and HMR-spectroscopy at 3.0T in the differential diagnosis of recurrent or residual gliomas: a comparative study. *Journal of Neuro-Oncology*. 2004;70(1):49–58.
95. Kyousuke K, Kiyohiro H, Hiroshi A, et al. Differentiation of cerebral radiation necrosis from tumor recurrence by proton magnetic resonance spectroscopy. *Neurologia Medico-Chirurgica*. 1997;37(3):250–256.
96. Sundgren PC. MR Spectroscopy in Radiation Injury. *AJNR Am J Neuroradiol*. 2009;30(8):1469–1476.
97. Rabinov JD, Lee PL, Barker FG, et al. In Vivo 3-T MR spectroscopy in the distinction of recurrent glioma versus radiation effects: initial experience1. *Radiology*. 2002;225(3):871–879.
98. Estève F, Rubin C, Grand S, et al. Transient metabolic changes observed with proton MR spectroscopy in normal human brain after radiation therapy. *International Journal of Radiation Oncology*Biology*Physics*. 1998;40(2):279–286.
99. Kaminaga T, Shirai K. Radiation-induced brain metabolic changes in the acute and early delayed phase detected with quantitative proton magnetic resonance spectroscopy. *Journal of Computer Assisted Tomography*. 2005;29(3):293–297.
100. Wald L, Nelson S, Day M, et al. Serial proton magnetic resonance spectroscopy imaging of glioblastoma multiforme after brachytherapy. *J Neurosurg*. 1997;87(4):525–534.

101. Tzika AA, Zarifi MK, Goumnerova L, et al. Neuroimaging in Pediatric Brain Tumors: Gd-DTPA-enhanced, Hemodynamic, and Diffusion MR Imaging Compared with MR Spectroscopic Imaging. *AJNR Am J Neuroradiol*. 2002;23(2):322–333.
102. Centers for Medicare & Medicaid Services (CMS (2004)). Decision memo for magnetic resonance spectroscopy for brain tumors (CAG-00141N). Baltimore, MD: CMS2004. Available at: http://www.cms.gov/medicare-coverage-database/details/nca-decision-memo.aspx?NCAId=52&fromdb=true.
103. Ricci P, Karis J, Heiserman J, et al. Differentiating recurrent tumor from radiation necrosis: time for re- evaluation of positron emission tomography? *AJNR Am J Neuroradiol*. 1998;19(3):407–413.
104. Di Chiro G, Oldfield E, Wright D, et al. Cerebral necrosis after radiotherapy and/or intraarterial chemotherapy for brain tumors: PET and neuropathologic studies. *Am J Roentgenol*. 1988;150(1):189–197.
105. Valk PE, Budinger TF, Levin VA, et al. PET of malignant cerebral tumors after interstitial brachytherapy : Demonstration of metabolic activity and correlation with clinical outcome. *Journal of Neurosurgery*. 1988;69(6):830–838.
106. Kim EE, Chung SK, Haynie TP, et al. Differentiation of residual or recurrent tumors from post-treatment changes with F-18 FDG PET. *Radiographics*. 1992;12(2):269–279.
107. Gómez-Río M, Rodríguez-Fernández A, Ramos-Font C, et al. Diagnostic accuracy of Thallium-SPECT and F-FDG-PET in the clinical assessment of glioma recurrence. *European Journal of Nuclear Medicine and Molecular Imaging.* 2008;35(5):966–975.
108. Janus T, Kim E, Tilbury R, et al. Use of [18F]fluorodeoxyglucose positron emission tomography in patients with primary malignant brain tumors. *Ann Neurol*. 1993;33(5):540–548.
109. Meyer MA, Frey KA, Schwaiger M. Discordance between F-18 fluorodeoxyglucose uptake and contrast enhancement in a brain abscess. *Clin Nucl Med*. 1993;18(8):682–684.
110. Witte OD, Goldberg I, Wikler D, et al. Positron emission tomography with injection of methionine as a prognostic factor in glioma. *J Neurosurg*. 2001;95(5):746–750.
111. Li Dong-li XY-k, Wang Quan-shi, WU Hu-bing, et al. 11C-methionine and 18F-fluorodeoxyglucose positron emission tomography/CT in the evaluation of patients with suspected primary and residual/recurrent gliomas. *Chinese Medical Journal*. 2012;Vol 125:091–096.
112. Van Laere K, Ceyssens S, Van Calenbergh F, et al. Direct comparison of 18F-FDG and 11C-methionine PET in suspected recurrence of glioma: sensitivity, inter-observer variability and prognostic value. *European Journal of Nuclear Medicine and Molecular Imaging.* 2005;32(1):39–51.
113. June-Key Chung YK, Seok-ki Kim, Yong Lee, et al. Usefulness of 11C-methionine PET in the evaluation of brain lesions that are hypo- or isometabolic on 18F-FDG PET. *European Journal of Nuclear Medicine and Molecular Imaging.* 2002;29(2):176–182.
114. Chen W, Silverman DHS, Delaloye S, et al. 18F-FDOPA PET imaging of brain tumors: comparison study with 18F-FDG PET and evaluation of diagnostic accuracy. *Journal of Nuclear Medicine*. 2006;47(6):904–911.
115. Yoshii Y, Satou M, Yamamoto T, et al. The role of thallium-201 single photon emission tomography in the investigation and characterisation of brain tumours in man and their response to treatment. *Eur J Nucl Med.* 1993;20(1):39–45.
116. Tie J, Gunawardana DH, Rosenthal MA. Differentiation of tumor recurrence from radiation necrosis in high-grade gliomas using 201Tl-SPECT. *Journal of Clinical Neuroscience.* 2008;15(12):1327–1334.
117. Vos M, Tony B, Hoekstra O, et al. Systematic review of the diagnostic accuracy of 201Tl single photon emission computed tomography in the detection of recurrent glioma. *Nucl Med Commun*. 2007;28(6):431–439.
118. Lamy-Lhullier C, Dubois F, Blond S. Lecouffe P, Steinling M. Importance of cerebral tomoscintigraphy using technetium-labeled sestamibi in the differential diagnosis of current tumor vs. radiation necrosis in subtentorial glial tumors in the adult. *Neurochirurgie.* 1999;45(2):110–117.
119. Henze M, Mohammed A, Schlemmer H, et al. Detection of tumour progression in the follow-up of irradiated low-grade astrocytomas: comparison of 3-iodo-a-methyl–tyrosine and 99mTc-MIBI SPET. *European Journal of Nuclear Medicine and Molecular Imaging.* 2002;29(11):1455–1461.
120. Palumbo B, Lupattelli M, Pelliccioli G, et al. Association of 99mTc-MIBI brain SPECT and proton magnetic resonance spectroscopy (1H-MRS) to assess glioma recurrence after radiotherapy. *The Quarterly Journal of Nuclear Medicine and Molecular Imaging.* 2006;50(1):88–93.
121. Jeune F, Dubois F, Blond S, Steinling M. Sestamibi technetium-99m brain single-photon emission computed tomography to identify recurrent glioma in adults: 201 studies. *Journal of Neuro-Oncology*. 2006;77(2):177–183.
122. Mountz J, Rosenfeld S, Li Y. Utility of T1–201 and Tc-99m-sestamibi SPECT for early determination of malignant tumor chemotherapy efficacy. *J Nucl Med*. 1993;34:89.
123. Sukanta B, Bandopadhayaya GP, Julka PK, et al. Imaging using Tc99m-tetrofosmin for the detection of the recurrence of brain tumour: A comparative study with Tc99m-glucoheptonate. *Journal of Postgraduate Medicine.* 2004;50(2):89–93.
124. Alexiou G, Fotopoulos A, Papadopoulos A, et al. Evaluation of brain tumor recurrence by (99m)Tc-tetrofosmin SPECT: a prospective pilot study. *Annals of Nuclear Medicine.* 2007;21(5):293–298.
125. Barai S, Rajkamal, Bandopadhayaya GP, et al. Thallium-201 versus Tc99m-glucoheptonate SPECT for evaluation of recurrent brain tumours: a within-subject comparison with pathological correlation. *Journal of Clinical Neuroscience.* 2005;12(1):27–31.
126. Samnick S, Bader JB, Hellwig D, et al. Clinical value of iodine-123-alpha-methyl-L-tyrosine single-photon emission tomography in the differential diagnosis of recurrent brain tumor in patients pretreated for glioma at follow-up. *Journal of Clinical Oncology*. 2002;20(2):396–404.
127. Kuwert T, Woesler B, Morgenroth C, et al. Diagnosis of recurrent glioma with SPECT and Iodine-123-α-Methyl tyrosine. *Journal of Nuclear Medicine*. 1998;39(1):23–27.
128. Floeth F, Pauleit D, Wittsack H, et al. Multimodal metabolic imaging of cerebral gliomas: positron emission tomography with [18F]fluoroethyl-L-tyrosine and magnetic resonance spectroscopy. *J Neurosurg.* 2005;102(2):318–327.
129. Verma R, Zacharaki EI, Ou Y, et al. Multiparametric tissue characterization of brain neoplasms and their recurrence using pattern classification of MR images. *Academic Radiology*. 2008;15(8):966–977.
130. Hu X, Wong KK, Young GS, et al. Support vector machine multiparametric MRI identification of pseudoprogression from tumor recurrence in patients with resected glioblastoma. *Journal of Magnetic Resonance Imaging.* 2011;33(2):296–305.
131. Blanchet L, Krooshof PWT, Postma GJ, et al. Discrimination between metastasis and glioblastoma multiforme based on morphometric analysis of MR images. *American Journal of Neuroradiology*. 2011;32(1):67–73.
132. Georgiadis P, Cavouras D, Kalatzis I, et al. Improving brain tumor characterization on MRI by probabilistic neural networks and non-linear transformation of textural features. *Comput Methods Prog. Biomed.* 2008;89(1):24–32.

133. Georgiadis P, Cavouras D, Kalatzis I, et al. Enhancing the discrimination accuracy between metastases, gliomas and meningiomas on brain MRI by volumetric textural features and ensemble pattern recognition methods. *Magnetic resonance imaging.* 2009;27(1):120–130.

134. Zacharaki EI, Wang S, Chawla S, et al. Classification of brain tumor type and grade using MRI texture and shape in a machine learning scheme. *Magnetic Resonance in Medicine.* 2009;62(6):1609–1618.

135. Joshi DM, Rana NK, Misra VM. Classification of Brain Cancer using Artificial Neural Network. Paper presented at: Electronic Computer Technology (ICECT), 2010 International Conference on; 7–10 May 2010, 2010.

136. Kassner A, Thornhill RE. Texture analysis: a review of neurologic MR imaging applications. *American Journal of Neuroradiology*. 2010;31(5):809–816.

137. Huang J, Wang A-M, Shetty A, et al. Differentiation between intra-axial metastatic tumor progression and radiation injury following fractionated radiation therapy or stereotactic radiosurgery using MR spectroscopy, perfusion MR imaging or volume progression modeling. *Magnetic Resonance Imaging.* 2011;29(7):993–1001.

138. Ando K, Ishikura R, Nagami Y, et al. Usefulness of Cho/Cr ratio in proton MR spectroscopy for differentiating residual/recurrent glioma from non-neoplastic lesions. *Nippon Igaku Hoshasen Gakkai Zasshi.* 2004;64(3):121–126.

139. Elias AE, Carlos RC, Smith EA, et al. MR spectroscopy using normalized and non-normalized metabolite ratios for differentiating recurrent brain tumor from radiation injury. *Academic Radiology.* 2011;18(9):1101–1108.

140. Traber F, Block W, Flacke S, et al. 1H-MR Spectroscopy of brain tumors in the course of radiation therapy: Use of fast spectroscopic imaging and single-voxel spectroscopy for diagnosing recurrence. *Rofo.* 2002;174(1):33–42.

141. Popperl G, Gotz C, Rachinger W, et al. Value of O-(2-[18F]fluoroethyl)-L-tyrosine PET for the diagnosis of recurrent glioma. *European Journal of Nuclear Medicine and Molecular Imaging.* 2004;31(11):1464–1470.

142. Rachinger W, Goetz C, Popperl G, et al. Positron emission tomography with O-(2-[18F]fluoroethyl)-l-tyrosine versus magnetic resonance imaging in the diagnosis of recurrent gliomas. *Neurosurgery.* 2005;57(3):505–511.

143. Terakawa Y, Tsuyuguchi N, Iwai Y, et al. Diagnostic accuracy of 11C-Methionine PET for differentiation of recurrent brain tumors from radiation necrosis after radiotherapy. *Journal of Nuclear Medicine*. 2008;49(5):694–699.

144. Tsuyuguchi N, Takami T, Sunada I, et al. Methionine positron emission tomography for differentiation of recurrent brain tumor and radiation necrosis after stereotactic radiosurgery–in malignant glioma. *Ann Nucl Med.* 2004;18(4):291–296.

145. Kline J, Noto R, Glantz M. Single-photon emission CT in the evaluation of recurrent brain tumor in patients treated with gamma knife radiosurgery or conventional radiation therapy. *AJNR Am J Neuroradiol*. 1996;17(9):1681–1686.

146. Yamamoto Y, Nishiyama Y, Toyama Y, et al. 99mTc-MIBI and 201Tl SPET in the detection of recurrent brain tumours after radiation therapy. *Nucl Med Commun.* 2002;23(12):1183–1190.